ktu
1922

Kaunas University of Technology

Faculty of Mechanical Engineering and Design

Evaluation of Negative Poisson's Ratio's Effect on 3D Printing

Master's Final Degree Project

Edgaras Polevičius

Project author

Assoc. Prof. Inga Skiedraitė

Supervisor

Kaunas, 2023

ktu
1922

Kaunas University of Technology

Faculty of Mechanical Engineering and Design

Evaluation of Negative Poisson's Ratio Effect on 3D Printing
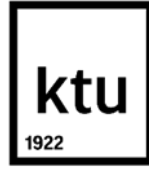
Master's Final Degree Project

Industrial Engineering and Management (6211EX018)

Edgaras Polevičius

Project author

Assoc. Prof. Inga Skiedraitė

Supervisor

Prof. Alvydas Kondratas

Reviewer

Kaunas, 2023

Kaunas University of Technology

Faculty of Mechanical Engineering and Design

Edgaras Polevičius

Evaluation of Negative Poisson's Ratio's Effect on 3D Printing

Declaration of Academic Integrity

I confirm the following:

1. I have prepared the final degree project independently and honestly without any violations of the copyrights or other rights of others, following the provisions of the Law on Copyrights and Related Rights of the Republic of Lithuania, the Regulations on the Management and Transfer of Intellectual Property of Kaunas University of Technology (hereinafter – University) and the ethical requirements stipulated by the Code of Academic Ethics of the University;

2. All the data and research results provided in the final degree project are correct and obtained legally; none of the parts of this project are plagiarised from any printed or electronic sources; all the quotations and references provided in the text of the final degree project are indicated in the list of references;

3. I have not paid anyone any monetary funds for the final degree project or the parts thereof unless required by the law;

4. I understand that in the case of any discovery of the fact of dishonesty or violation of any rights of others, the academic penalties will be imposed on me under the procedure applied at the University; I will be expelled from the University and my final degree project can be submitted to the Office of the Ombudsperson for Academic Ethics and Procedures in the examination of a possible violation of academic ethics.

Edgaras Polevičius

Confirmed electronically

Kaunas University of Technology

Faculty of Mechanical Engineering and Design

Task of the Master's Final Degree Project

Given to the student – Edgaras Polevičius

1. Title of the Project

Evaluation of Negative Poisson's Ratio's Effect on 3D Printing
(In English)

Neigiamo Puasono santykio poveikio 3D spausdinimui įvertinimas
(In Lithuanian)

2. Aim and Tasks of the Project

Aim: to evaluate mechanical and economical benefits a negative Poisson's ratio on 3D printing.
Tasks:
1. to analyze applications of a negative Poisson's ratio;
2. to compare different 3D printable structures exhibiting a negative Poisson's ratio;
3. to test mechanical properties of auxetic 3D printed structures;
4. to review economic viability of applying auxetic structures in AM.

3. Main Requirements and Conditions

Requirements: structures under investigation should be a 5x3 pattern, with varying wall thicknesses from 0.45 to 2.25 mm, by increments of 0.45 mm.
Parameters to be achieved: Young's modulus, compressive strength and cost for printed parts.

4. Additional Requirements for the Project, Report and its Annexes

"Not applicable"

Project author	Edgaras Polevičius		2023 03 03
	(Name, Surname)	*(Signature)*	*(Date)*
Supervisor	Inga Skiedraitė		2023 03 03
	(Name, Surname)	*(Signature)*	*(Date)*
Head of study field programs	Regita Bendikienė		2023 03 03
	(Name, Surname)	*(Signature)*	*(Date)*

Summary

The project encompassed an investigation upon auxetic and hexagonal structures, which are two types of lattice structures that have attracted significant attention in recent years. Both structures have unique mechanical properties that make them ideal for various applications, including aerospace, medical devices, and sports equipment. The auxetic structure is characterized by a negative Poisson's ratio, making it expand in the transverse direction when stretched in the axial direction. In contrast, the hexagonal structure has a positive Poisson's ratio, which means that it contracts in the transverse direction when stretched in the axial direction. The auxetic structure is known for its exceptional energy absorption ability, while the hexagonal structure is known for its high stiffness and strength. To further investigate the mechanical properties of the structures, SolidWorks software was used to simulate their behaviour under compression. The simulations indicated that the auxetic structure had a more uniform stress distribution compared to the hexagonal structure. To compare the mechanical properties of these structures, compression tests were performed using a universal testing machine, after 3D printing them using an FDM printer. The results showed that the auxetic structure had a higher compressive strain compared to the hexagonal structure. This can be attributed to the unique deformation mechanism of the auxetic structure, which involves the rotation of the unit cells. The hexagonal structure, on the other hand, deformed through bending and stretching of the unit cells. Based on the performed cost analysis, it was concluded that the choice between the auxetic and hexagonal structures depends on the specific application requirements. If high energy absorption capacity and resistance to localized failure are critical, then the auxetic structure would be a better option. However, for high stiffness and strength the hexagonal structure would be a better option. By comparing their mechanical properties and printing characteristics, the advantages and disadvantages of each structure were highlighted, and insight were provided into their cost-effectiveness.

Santrauka

Projektas apėmė auksetinių ir šešiakampių struktūrų, kurioms pastaraisiais metais skiriama daug dėmesio, - tyrimą. Abi struktūros pasižymėjo unikaliomis mechaninėmis savybėmis, todėl puikiai tinka įvairiems pritaikymams, įskaitant aviacijos, medicinos prietaisus ir sporto įrangą. Auksetinėms struktūroms yra būdingas neigiamas Puasono santykis, todėl tempiama ašine kryptimi ji plečiasi skersine kryptimi. Šešiakampės struktūros Poisono santykis yra teigiamas, tai reiškia, kad tempiama ašine kryptimi ji susitraukia skersine kryptimi. Auksetinė struktūra pasižymėjo išskirtiniu energijos sugėrimo pajėgumu, o šešiakampė struktūra - dideliu standumu ir stiprumu. Siekiant išsamiau ištirti konstrukcijų mechanines savybes, jų elgsenai gniuždant modeliuoti buvo naudota "SolidWorks" programinė įranga. Modeliavimas parodė, kad auksetinė struktūra, palyginti su šešiakampe struktūra, pasižymi tolygesniu įtempių pasiskirstymu. Šių struktūrų mechaninėms savybėms palyginti buvo atlikti gniuždymo bandymai naudojant universalią bandymo mašiną, po to, kai jos buvo atspausdintos 3D FDM spausdintuvu. Rezultatai parodė, kad auksetinė struktūra pasižymėjo didesne gniuždymo deformacija, palyginti su šešiakampe struktūra. Tai galima paaiškinti unikaliu auksetinės struktūros deformacijos principu, kuris apima vienetinių elementų sukimąsi. Kita vertus, šešiakampė struktūra deformuojasi dėl vienetinių elementų lenkimo ir tempimo. Remiantis atlikta sąnaudų analize, buvo padaryta išvada, kad pasirinkimas tarp auksetinės ir šešiakampės struktūros priklauso nuo konkrečių pritaikymo reikalavimų. Jei labai svarbu didelė energijos sugertis ir atsparumas lokaliems susilpnėjimams, tuomet geresnis variantas būtų auksetinė struktūra. Tačiau jei reikia didelio standumo ir stiprumo, geresnis variantas būtų šešiakampė struktūra. Palyginus jų mechanines savybes ir spausdinimo charakteristikas, buvo atskleisti kiekvienos struktūros privalumai ir trūkumai bei pateikta įžvalga apie jų ekonominį efektyvumą.

Table of Contents

List of Figures

List of Tables

Introduction

The project comparing auxetic and hexagonal structures is a relevant and novel approach to exploring the properties of 3D printed materials. As AM continues to advance, it becomes increasingly important to investigate the unique characteristics of different 3D printed structures. This project aims to compare two specific types of 3D printed structures, auxetic and hexagonal, in terms of their compression strength and cost benefit. The relevance of this project lies in the potential practical applications of 3D printed structures in a variety of fields, including aerospace, automotive, and biomedical engineering. Understanding the properties of these structures can lead to the development of new and innovative designs that can improve the efficiency and effectiveness of various products. The practical results of this project can have significant implications for various industries. For example, in the aerospace industry, auxetic and hexagonal structures can be used to design lightweight and strong components for aircraft and spacecraft, which can improve fuel efficiency and reduce costs. In the automotive industry, these structures can be used to design crash-absorbing components, reducing the risk of injury to passengers in the event of a collision. In the biomedical field, auxetic and hexagonal structures can be used in the development of prosthetics and implants, which require both strength and flexibility. Furthermore, the use of the project 's cost-benefit analysis can also provide insights into the economic feasibility of using auxetic versus hexagonal structures in engineering applications. By comparing the cost of manufacturing of both of these structures to the benefits gained from their improved mechanical properties, it could be determined if their use is a viable economic decision in various industries. The reduction in material usage associated with auxetic structures can have a positive impact on the environment. This is because the production of traditional materials often requiring substantial amounts of energy and generating significant amounts of waste. By reducing material usage, auxetic structures can help to minimize the environmental impact of manufacturing processes. The use of 3D printing technology in this project can help to advance the field of additive manufacturing, also serve as an insight for peers in the scientific community who are interested in the mechanical, economical and geometrical properties of innovative new meta-materials and structures. It could inspire further research and innovation in the field of materials science and engineering. By exploring the performance of several types of structures, this project can help to inform future research and development efforts aimed at improving 3D printing technology. Overall, this project has the potential to contribute to the advancement of 3D printing technology and provide valuable insights into the properties of different 3D printed structures, by filling in the gaps in lacking research areas. It also has practical implications for a variety of industries, making it a relevant and key area of research in terms of a reduced environmental impact. It could lead to the development of new materials, contribute to the development of sustainable engineering solutions, and inform the design of engineering structures across a range of fields.

Aim: to evaluate mechanical and economical benefits a negative Poisson's ratio on 3D printing.
Tasks:
1. to analyse applications of a negative Poisson's ratio;
2. to compare different 3D printable structures exhibiting a negative Poisson's ratio;
3. to test mechanical properties of auxetic 3D printed structures;
4. to review economic viability of applying auxetic structures in AM.

Hypothesis: would an increase in wall thickness of an auxetic structure yield better results than a hexagonal structure?

1. Analysis of Applications of NPR

Materials and structures possessing a negative Poisson's ratio, otherwise known as auxetic, have gained an increased interest over the last decade, due to the mechanical benefits they present in a variety of industries. Conducting a citation report using Web of Science's reference and citation database it was found that the number of publications and citations related to the term "negative Poisson's ratio" have increased exponentially since 2011, as shown in Fig. 1.
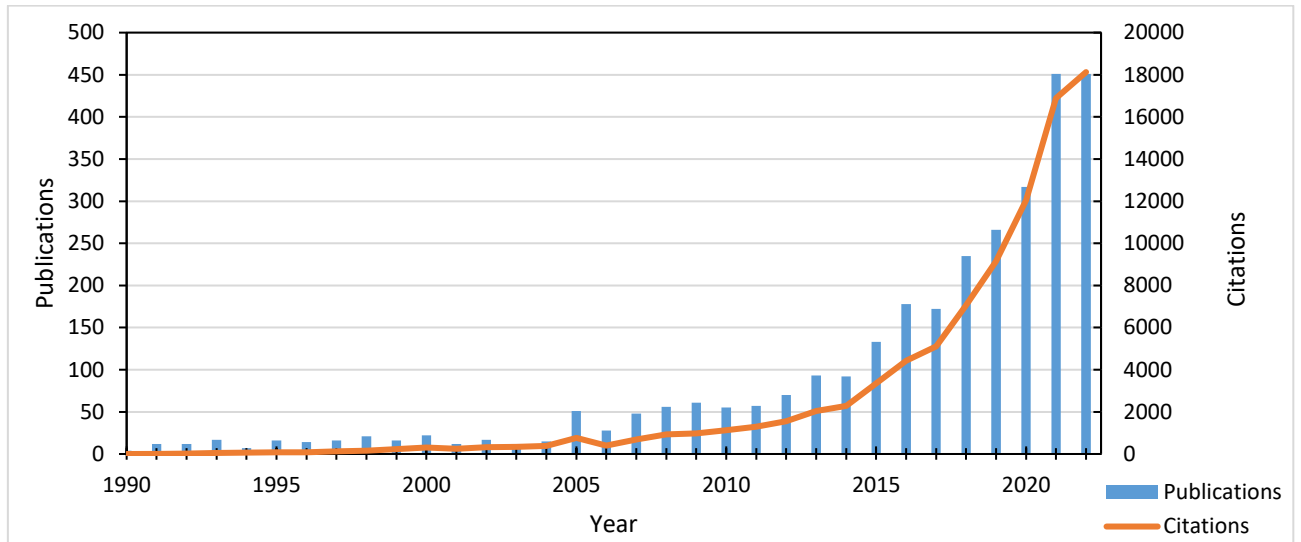
Fig. 1. Number of publications, citations per year (during 1990-2022), data obtained from Web of Science

These relatively recently appointed mechanical metamaterials have been under investigation to acquire the necessary mechanical performance as well as secondary beneficial attributes not typically found in conventional structures and materials. These ventures in material science contribute to contemporary breakthroughs in aviation, military, medicine, robotic industries [1].

Benefits of impact resistance can be gained from structural examples presented in nature's biological materials or organisms and applied to manufacturing protective equipment, body, and head armour [2], for example analysing a conch shells architecture [3]. These developments have a high value to protective sports gear, as preventative measures taken to preserve the health of athletes are exponentially cheaper than treatment in case of long-term injuries [4]. Examples of these are shown in Fig. 2.

Fig. 2. Wearable protective equipment for: a) knees [5], b) arms [6]

As the most extreme sports are considered contact and collision types, such as boxing, football, hockey, etc., protective gear is required to be highly resistive to impact, penetration and be energy

absorbent, therefore material of traditional protective gear is evaluated to eventually be superseded by more mechanically sound alloys [7]. This becomes crucial in protective military gear, as each miniscule improvement yields the prevention of attaining a critical injury or death. For combat measure materials such as titanium alloy, alloy steel, nylon, aramid, and ultrahigh molecular weight polyethylene are used currently and have been investigated in a study [8], which proves that headgear with a rectangular shell structural pattern is able to absorb the biggest impact force. Similarly, headgear was investigated when inserting auxetic foams , shown in Fig. 3. While strict resistance to ballistics is a key concern for these fields, such considerations as comfort, weight and flexibility are only a secondary concern and does not have the amount of research on them in comparison.
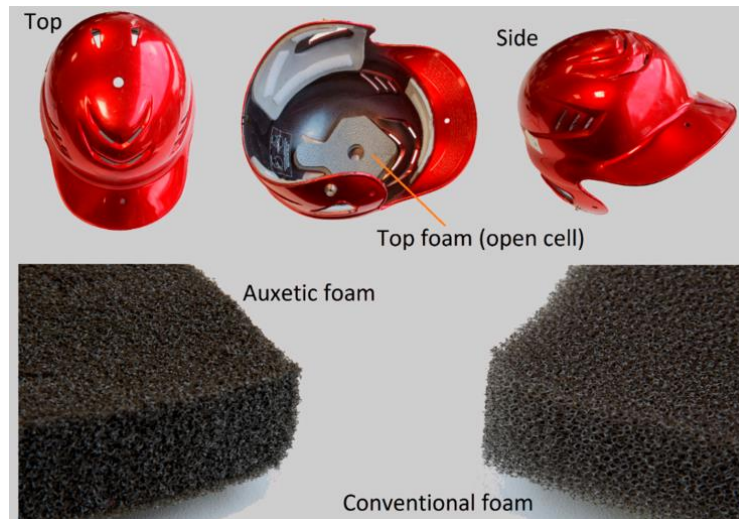
Fig. 3. Example of auxetic foam inserts inside protective headgear

Mechanical flexibility presented in metamaterials allows for structures which are superior and not typically found in nature, which are suitable for innovative optical instruments [9]. A negative Poisson's ratio in device components, can provide use in the design of diffraction gratings in optical instruments, which are used to control and split light. Typically, these gratings are made of flat sheets of material with closely spaced parallel lines or grooves etched onto them. These grooves function as small optical components that can reflect or diffract light in a controlled manner. However, by incorporating auxetic materials into the design of these gratings, they can offer greater control over the intensity and direction of the diffracted light.

Continuing the observation from a medical point of view analysing applications of materials inhibiting a negative Poisson's ratio is fitting due to human tissues highlighting auxetic tendencies [10, 11]. Auxetic bioengineered tissues are used in reconstructive surgery for various body parts: skin, bone, artery, tendons [12]. For example, there has been an interest even in less critical operations, such as using mesh implants for inguinal hernia repair [13]. Auxetic structures can be used in the development of prosthetic devices due to their exceptional mechanical properties, such as flexibility, stability, and durability, examples shown in Fig. 4. Breakthroughs could be achieved in the development of implants, particularly in orthopedics, due to their exceptional mechanical properties, such as, using auxetic structures to create artificial joints, which can provide greater stability and range of motion compared to traditional implants.
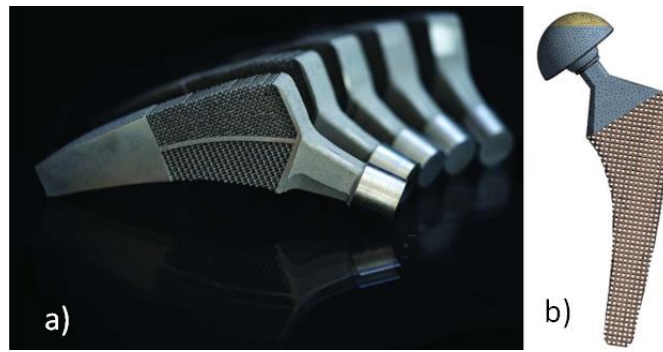
Fig. 4. Examples of implants possessing NPR structures: a) hip implant [14], b) femur [15]

Another use was shown in the form of a 3D printed treatment garments [16]. Additionally, auxetic structures can be used to create artificial bones, which can provide greater strength and durability compared to traditional materials. However, when working with organic material, especially that of a human's, the main concerns of related investigations are that of the tissue's compatibility with that of a patient, its cellular attachment capabilities, resistance to diseased cells. Further work needs to be done on the artificials tissue's performance under dynamic load to prove to be a viable long term restorative medical solution.

Analogically to mimicking existing human structures, metamaterials can be used in furthering robotics. Auxetic and non-auxetic combinations were explored to be useful in soft robotics [17]. Soft robots are robots that are composed of soft and flexible materials, such as rubber or silicone. These robots have gained popularity due to their ability to mimic the natural movements of living organisms, which makes them ideal for use in various applications, such as in medical devices or rescue robots. Auxetics can be utilized for their localized deformation and be used in confined spaces, such as rescue missions under hardly accessible debris, interplanetary probes for efficient traversal of rough terrain., NPR structured springs were utilized for a robot's legs [18], shown in Fig. 5, which provides a potential 35.2% increase in energy than using a corresponding conventional spring. This means that auxetic structures can be used to create flexible joints for the soft robots, which can provide a greater range of motion and movement compared to traditional robots.
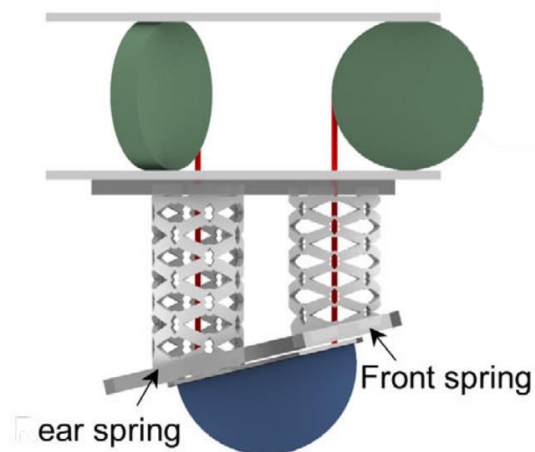
Fig. 5. Robot leg utilizing auxetic sprigs [18]

Correspondingly, these structures can also provide better stability and control, allowing the soft robots to move more efficiently and accurately. Combining these attributes with exoskeletons, would

enhance the physical capabilities of humans. These devices can be used to assist individuals with mobility impairments, such as those who have suffered a spinal cord injury or stroke, to walk and perform other activities. Auxetic structures can be used to create flexible joints and components for the exoskeleton, which can provide greater mobility and comfort to the user. Large bending deformations were discovered to be more feasible as well as a bonus larger capacitive charge and improved sensitivity in sensors, which would allow for improved grippers used in robotics [19], which would yield use in applications were traditional, hard grippers would be too damaging or too imprecise. In contrast to the standard sensor architecture, which causes the width of the sensor to decrease, the suggested sensor configuration makes use of auxetic structures with a negative Poisson's ratio to widen the sensor in response to the major strain in the length direction. The sensor's deformation features lead to increased sensitivity and a bigger capacitive change. It was demonstrated through characterization that the manufactured sensors have enhanced sensitivity—roughly two times that of the typical sensors. NPR structures can be used to create the flexible fingers of these grippers, which can bend and conform to the shape of the object being grasped, providing a more secure and precise grip . For mobility purposes, similar benefits could be utilized and applied to wearable smart devices, monitoring body systems and undergoing substantial constant strain for highly stretched skin areas, shown in Fig. 6 [20]. The structure that is produced by mapping unit cells with various Poisson's ratios to the target surface will have the same mechanical characteristics and deformation behavior as the skin it is covering. As a result, the connection points between wearable electronics and human skin would experience less shear stress, increasing the durability of the attachment. Additionally, the device's conformability might be produced.
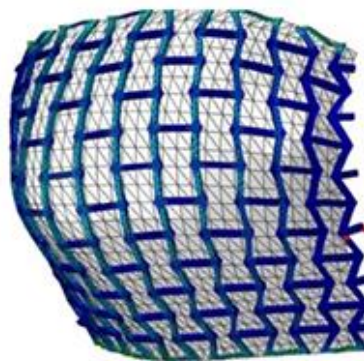
Fig. 6. FEA model of a structure's conformability [20]

Additionally, structures with a NPR have the capability to be utilized in filtration systems, due to the structures possessing open porous geometry. Filter systems are used in various areas, such as water processing facilities, air filtration, and oil filtration, to remove contaminants and impurities from the fluids. Among the analysed structures, the most consistent NPR possessing structures were concluded to be most suitable for air, water filtration systems [21]. Actual experiments were conducted on auxetic foams via a tensometer machine [22], which led to results displaying a 50% decrease for air pressure drops, when under tensile strain, compared to the regular foams possessing just a constant drop. A compound fabric for the uses of transportation and filtration was produced from a conventional fabric [23]. The filtration of particles utilizing auxetic structures cut into the fabric was achieved with the option of adjusting the slit sizes allowing particles of different proportions to pass through. However, it was noted that the larger the unit cell size, the lower mechanical properties. Consequently, higher unit cell sizes can be considered for particle filtration, taking into account applied tensile loads upon the structure.

A different field where the negative Poisson's ratio could be utilized in packaging. A proposal to introduce composite auxetic metamaterials towards crates was created [24]. The performed force absorption tests upon the hybrid structures proved to result in a ~140% increase in the factor of safety. This means that, boxes and wheels utilizing these arrays would prevent packaged inventory to potentially avoid higher amounts of breakage. A lithium-ion battery case was proposed [25], substantiated by axial impact experiments performed on multiple designs using machine learn methods. The result was an optimal case with the layout of an auxetic honeycomb, which showed highest energy absorbance capabilities.

Furthermore, one of the primary applications of auxetic structures in aerospace is in the development of lightweight and durable composites. Composites are materials that are made up of two or more varied materials, such as polymers and metals, which are combined to create a new material with improved properties. These types of materials utilizing a negative Poisson's ratio, were researched in terms of circular tubes [26], as presented in Fig. 7. In several fields, including the automotive, medical, pipeline, and aerospace industries, hybrid tubes of various types have been developed and utilized for protective gear, oesophageal stents, oil and gas pipelines, and high-quality vibration dampers.
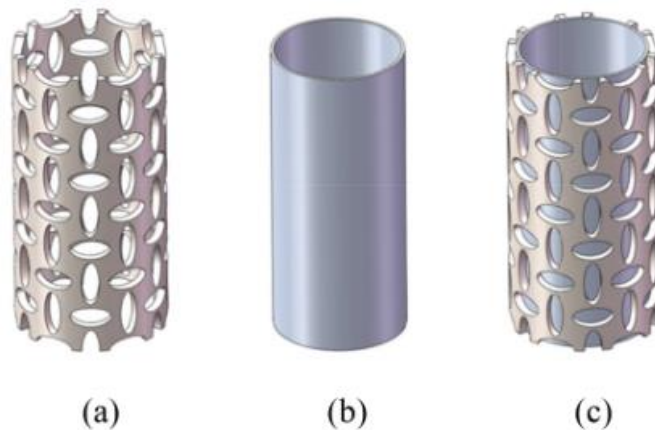
Fig. 7. Designs of: (a) auxetic tube; (b) conventional tube; and (c) hybrid tube [26]

The tested hybrid tubes presented highest ratio of crushing force to maximum force, as well as peak total energy absorption when compared to conventional tubes. By systematically extrude-cutting circular, oval and hybrid shapes into the tube, strategical removal of material could yield not only a more lightweight, energy saving but also potentially more aerodynamic and mechanically durable structure. By incorporating auxetic structures into the design of these structures, aerospace engineers can create supports that are stronger, lighter, and more flexible than traditional beams.

Another justified use of NPR structures in aerospace is in the development of aircraft components. These structures can be used to create composite materials that can withstand the extreme forces and stresses experienced by aircraft components, such as wings [27]. By using NPR structures in these components and potentially others, aircraft engineers can create parts, which would withstand larger displacement with restricted straining on the components, thus improving the overall performance and efficiency of the aircraft. In addition to their use in composites and aerospace components, auxetic structures can also be used in the development of energy-efficient smart materials for aerospace applications [28]. Morphing aircraft is a novel concept in the aerospace industry, describing vessels which utilize modern material science breakthroughs to allow for change of shape or configuration

during flight. Similarly, the core structure for a prototype airplane wing exhibited NPR behaviour [29], shown in Fig. 8. Likewise, these materials can be used in the development of thermal insulation materials, which are used to protect spacecraft and satellites from extreme temperature changes. By incorporating auxetic structures into silicon foams for the first time [30], a foam with over 80 times more energy dissipation than a conventional foam was produced with the additional features of low water absorption and thermal resistance. These materials could then be used in aerospace vessels walls, providing more robust thermal protection than concurrent foams.
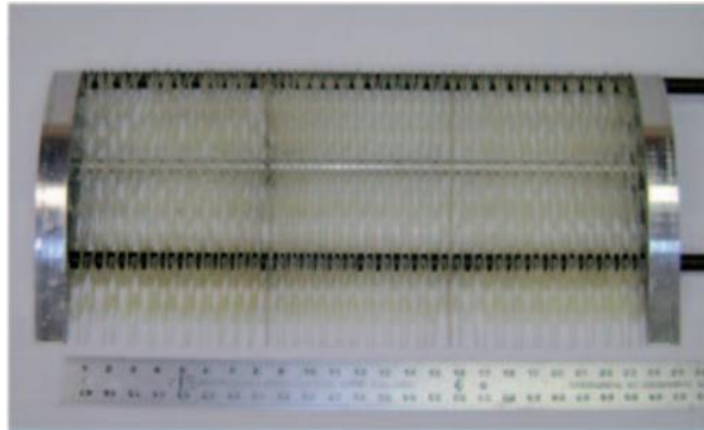
Fig. 8. Assembled core of a wing using auxetics [29]

In the field of architecture, NPR possessing structures have met success as well. Heat actuated auxetic facades were proposed as a solution [31]. A varied shading experiment was conducted to investigate the effect of heat upon auxetic cells, which causes the porous structure to either contract or expand. Consequently, compared to non-dynamic façade's the auxetic variant inhibited a better daylight performance of the tested space. Implementation benefits for architectural structures were displayed, by producing lightweight synclastic grid shells [32]. The proposed methodology also recommended using 3D printing as the most viable solution to customize, reconfigure 2D re-entrant grids used in mega-structures. These structures potentially could create large, open spaces with minimal material used in the process, which would lead to improved sustainability and reduced environmental impact.

Porous materials are widely used in contemporary construction of the latter systems, due to their passive energy absorption and dissipation, but have proved to have critical problems in terms of other mechanical features. An auxetic foam structure has been proven to not only yield higher shock energy dissipation capacity, but also higher resistance to impact force and better sound absorption [33]. As it was important of protective gear material to be relatively lightweight discussed previously, it is especially crucial to minimize it when it comes to aircraft engineering, as it is a viable solution towards fuel preservation. It was even proven that removing material in certain areas in a structure could have minimal to no loss of stability and other mechanical properties [34].

New 2D and 3D auxetic structures have only started to be under thorough investigation in the past 5 years [35, 36], with the main related research categories depicted in Fig. 9. Neglecting material sciences, most focus is projected on mechanical and physical capabilities, with other disciplines such as chemistry and nanoscience in subsequent statures. These presented more viable mechanical properties than before widely applied designs which benefit current material science progress towards more economical and robust components used in vehicles and aircraft [37].

17
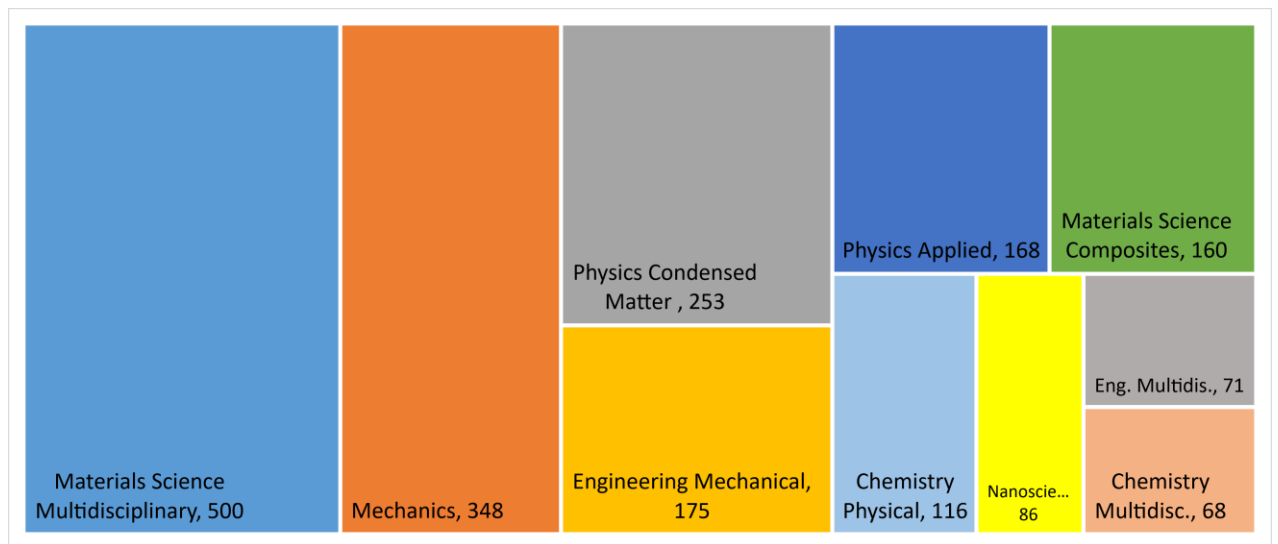
Fig. 9. Amount of "Negative Poisson's ratio" keyword used, by article categories, from Web of Science

The main drawback that auxetic structures indicate overall is their low stiffness when compared to conventional structures, as research centred around NPR [38], tends to find solutions to diminish this effect. The material's stiffness refers to how much it resists deforming when a force is applied. It stands for the material's capacity to endure pressure and keep its form. The material may flex more easily when a force is applied when it has a lower stiffness. It is more easily bent or stretched, and less power is needed to cause a certain degree of deformation. Less rigid materials are often more elastic, malleable, or flexible. Applying this to NPR structures in areas such as construction, vehicle production, aeronautics the before mentioned utilization as structural members of systems should be revaluated.

Another disadvantage of auxetic materials is their geometrical complexity. As additive manufacturing technologies get more implemented in various industries, NPR structures demonstrated challenges. Simple 2D patterns present no issue when it comes to 3D printing [39], however more intricate design features, as shown in Fig. 10 lead to increased print times, supporting structures, printing inaccuracies [40].
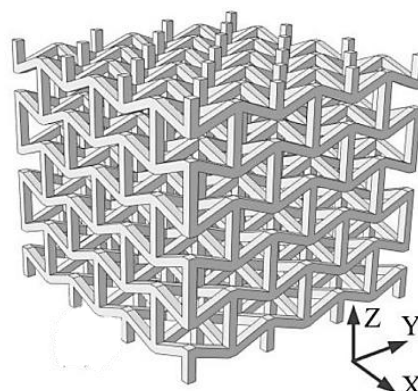
Fig. 10. 3D re-entrant auxetic structure [41]

Support structures may be necessary for complex constructions to maintain stability and stop sagging or collapsing during printing. To hold up overhanging or unsupported portions of the design, these support structures are required. The printing time, material use, and post-processing time necessary

to remove or clean up the supports, however, increase when support structures are included. The capabilities of the 3D printer, the printing process selected, and the material being utilized may all affect how fine of a detail may be produced. Complex designs may be difficult to copy correctly using low-resolution printers or materials with restricted detail reproduction. The strength and integrity of the finished printed product may be compromised by narrow channels, tiny gaps, or sophisticated interlocking elements that obstruct the flow of the printing material. As the intricacy of the design rises, it becomes increasingly crucial to guarantee optimum material flow and structural stability.

1.1. Summary of Analysis of Applications of NPR

What has been indeed lacking in the research of auxetic materials is the correlation between the mechanical benefits versus the economic advantages. For example, due to this particular material science area's recency, the general focus, experiments and tests have been set on mostly on the mechanical qualities, such as inherent structural properties [39, 41, 42, 43, 44], Young's modulus ratio and instability . Adequate insight has been lacking whether production of these 3D printed structures is actually cost-effective or even worth their relatively more intricate productions processes. Moreover, no insight was done into the relationship between material saved or even lost while creating negative Poisson's ratio structures and mechanical benefits gained as opposed to conventional structural methods. Lastly, not enough data has been presented whether utilizing these structures in wider scale operations to ensure that it would be a sound economic method.

2. Analysis of Structures Exhibiting a Negative Poisson's Ratio

Conventionally, structures that have a positive Poisson's ratio have the tendency to display Poisson's effect – the effect of a 2D structure or solid object to become thinner or decrease in its cross section when under longitudinal strain. Contrastingly, when a structure has a negative Poisson's ratio, the material tends to expand laterally when strained longitudinally, and lose cross sectional area when under compression [45]. Comparison of both cases is shown in Fig. 11.
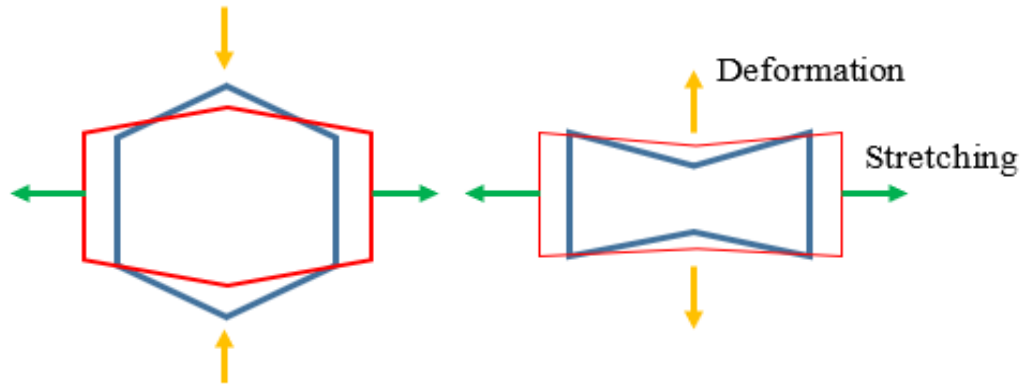
Fig. 11. Comparison between a non-auxetic (left) and an auxetic (right) structure cell

There is a wide array of different auxetic structures, the majority of which could be categorized into three main groups:

–   Rotating polygon auxetics
–   Re-entrant auxetics
–   Chiral auxetics

Rotating auxetic structures, otherwise known as the rotating polygon model's, main elements consist of polygons, usually squares [46], which are connected via hinges which and rotate about vertices, an example can be seen in Fig. 12.
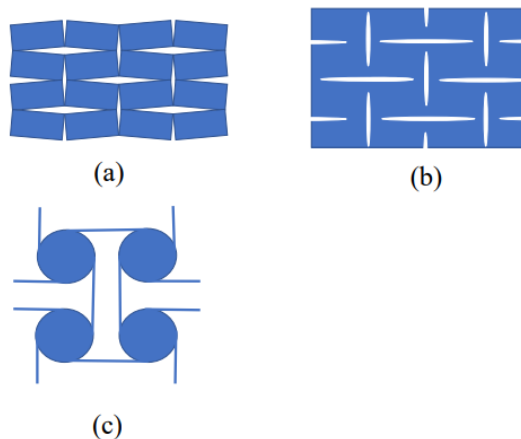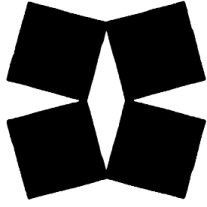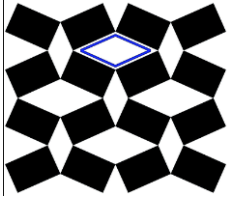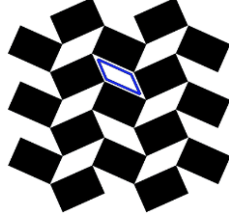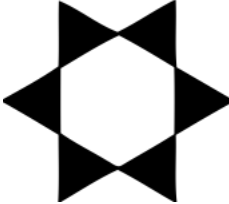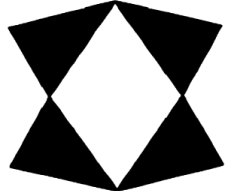
Fig. 12. Different rotational polygonal auxetic structures [46]: (a) opened rotating squares, (b) perforated sheet structure, (c) the anti-tetrachiral model

Auxetic properties of these models appear when they are assigned to the loads with uniaxial eccentricities, which causes rotation of polygons relative to each other and an increase of the size of the gaps between the cells, thus increasing the structures overall cross-section. Figure 9(b) shows the most simplistic pattern of this type, which is comprised out of equal, perpendicular horizontal and vertical slits. The initial unmodified structure, later to be emulated, is shown in Figure 9(a). Figure

20

9(c) highlights an extreme deviation from the initial designs, when more porosity is utilized. These interchangeable cells can be patterned and generated in various forms, based on required properties, available materials and the purpose. Main examples of rotating auxetic models were analysed and inserted into Table 1.

Table 1. The main shape variations of 2D rotational polygon auxetic structure models

Cell shape	Key features
Square	Always maintains aspect ratio, thus has constant Poisson's ratio of -1, under any loading direction. [46] [47].
Rectangle (rhombi lattice)	Poisson's ratio is influenced by ratio of the rectangle width and height, angle between rectangles, loading direction [48].
Rectangle (parallelogram lattice)	Structures with rhombi lattices have a Poisson's ratio of -1 [48].
Triangle (equilateral)	Always maintains aspect ratio, thus has constant Poisson's ratio of -1, under any loading direction. [49].
Triangle (isosceles)	Can have negative or positive Poisson's ratio, depending on the shape of the triangles, angles between them, ratio between the two equal sides and the odd side. [48].

Despite these more widely used patterns there are still more structural types which could be used. For example, the interlinked polygons could be also pentagons, hexagons, etc, and not necessarily consist of only regular shapes. In fact, the grid can be substituted with more lightweight connections [50], and even be generated from different shapes altogether. Differences made from the longer-lasting standardized patterns would need further, more complex calculations and tests to prove their inception. It can be deducted that, one of the advantages that these cell types offer over other auxetic

structure groups is that due to its grid pattern being comprised out of regular shapes it can offer tunability to its mechanical properties [48]. By having the option to change the shape, size, scale and array of the polygons it allows to pursue one or set of particular properties such as impact absorption, rigidness, stiffness and others. A dynamic approach was performed [51] by using controllable "intelligent hinges" between the polygons, which allows alteration of the Poisson's ratio via hinge resistance. Analysis of auxetic behaviour of rotating squares was analyzed [47]. A rotating polygon nanostructure was optimized by finding the best ratio between a rotating square unit cell's height and width [52]. Adjusting the geometry, the Poisson's ratio value was altered from a positive to a negative value and vice versa. Young's modulus was found to decrease as the ratio between the square's height and width increased.

Re-entrant, more categorically known as re-entrant honeycomb, auxetic structures are made up from interlinked cells, which are inward pointing. These shapes, also known as re-entrants, are polygons, having angles bigger than 180°. These structures were achieved by modifying a standard honeycomb structure [53], specifically changing the base polygon's shape into a concave hexagon resembling one. One of the main challenges is in designing and manufacturing these structures, which can be more complex than traditional materials due to their unique geometry. This can also be seen as an advantage, since when compared to traditional hexagonal forms with the same dimensions, re-entrant hexagonal structures often have a higher surface area. In applications like filtration, where a greater surface area permits improved filtering efficiency or adsorption capacity, the increased surface area might be advantageous. The particular parameters, such as the angle of re-entrancy or the size of the voids between links, can be changed to further customize the behaviour of re-entrant hexagonal formations. Due to its tunability, desired features, including the size of the negative Poisson's ratio or the range of deformation, may be optimized.

A different re-entrant shape from the typical ones, as presented in Fig. 13, are the star-shaped auxetics. are formed by taking a regular polygon and placing a smaller, similar polygon inside it, with vertices connected to the midpoints of the sides of the larger polygon [54]. This process is then repeated recursively, forming a star-shaped pattern with multiple layers of nested polygons. The resulting structure possesses a negative Poisson's ratio, allowing it to contract in the perpendicular direction under compression or stretching. The star-shaped re-entrant structure has a number of benefits over other types of auxetic structures. For example, it has a higher negative Poisson's ratio than other types of re-entrant structures, which means that it can contract more in the perpendicular direction under deformation. The structure has unique design that allows it to be easily customizable to specific applications. By changing the number of sides of the nested polygons, the size of the structure can be adjusted to suit different requirements. Moreover, by adjusting the relative sizes of the polygons, the material properties of the structure can be modified to optimize its performance for different applications [55]. However, the star-shaped re-entrant structure also has a set of drawbacks. Its complex design makes it more difficult to manufacture than other types of auxetic structures, such as the honeycomb structure. The number of nested polygons required to achieve the desired negative Poisson's ratio can lead to a high density of material, which can result in increased weight and reduced flexibility.
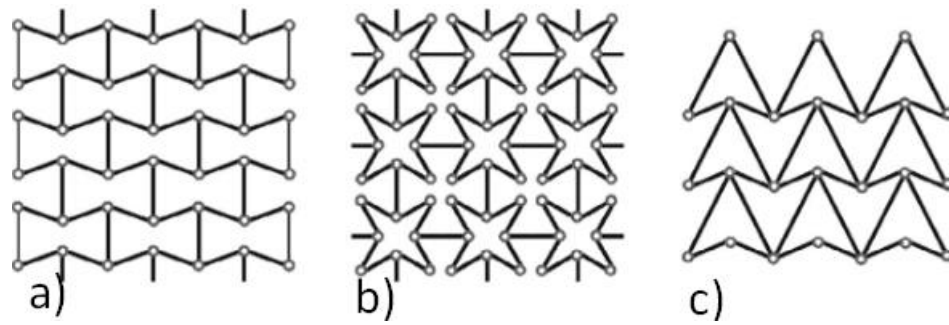
Fig. 13. Typical 2D re-entrant lattices: a) re-entrant hexagon, b) star-shaped, c) double arrowhead [56]

Double arrowhead structures derive their name from their shape, which looks like two arrowheads connected at their bases. The design is created by initiating with a rectangular unit cell and then eliminating two triangles from opposite corners, example shown in Fig. 14. This results in a structure that repeats in both directions, generating an interconnected pattern of arrowheads. One of the advantages of double arrowhead auxetics is that they exhibit a substantial negative Poisson's ratio, enabling them to contract in the perpendicular direction under stretching or compression. This feature is beneficial in minimizing deformation in applications like protective gear or medical devices. Furthermore, the double arrowhead design is highly flexible, which can be useful in applications requiring bending or flexing. Despite these benefits, there are also distinct disadvantages to using double arrowhead auxetics. The design is quite intricate, making it challenging to manufacture using traditional methods. Moreover, the structure's shape can result in stress concentrations in denser areas, leading to material failure under certain circumstances. To address these challenges, researchers have investigated using additive manufacturing methods, such as 3D printing, to create the structures with precision and control.
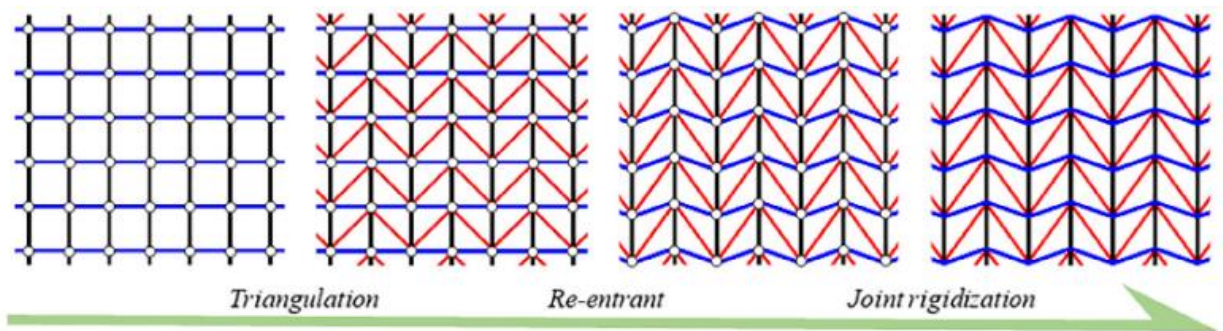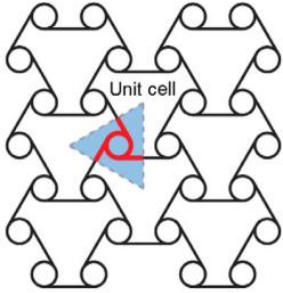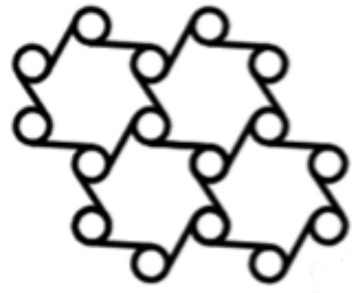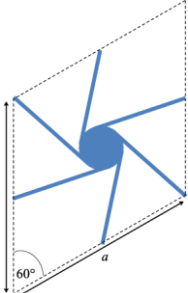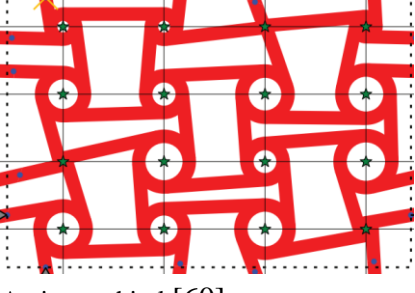
Fig. 14. Design of a 2D auxetic triangular framework [56]

Chiral auxetics are a class of materials that exhibit both auxetic and chiral properties. Chiral materials are those that lack mirror symmetry and exhibit distinct left-handed and right-handed forms. The combination of these two properties in chiral auxetics results in unique mechanical properties that make them potentially useful in a range of applications. Chiral patterns can be made from a variety of materials, including polymers, metals, and composites. They are typically fabricated using techniques such as 3D printing or electrospinning, which allow for precise control over their geometry and structure. One of the key features of chiral structures is their unique microstructure, which consists of a repeating pattern of helical or spiral-shaped units that interlock in a specific way, shown in Table 2.

Table 2. Common chiral auxetic structures

Cell shape	Key features
Anti-trichiral [57]	All of the ligaments develop plastic hinges when the honeycomb is crushed to significant distortion. May exhibit a positive or negative Poisson's ratio value, depending on compression applied.
Trichiral [58]	In-plane Poisson's ratio is −1. The Poisson's ratio of their system is maintained throughout a significant range of strain, in contrast to the majority of other negative Poisson's ratio materials.
Hexachiral [59]	Results show that, in contrast to other auxetic geometries, the hexachiral honeycomb system is exceptionally tolerant to translational disorder and has the capacity to maintain roughly its original Poisson's ratio despite degrees of disorder of up to 90%.
Anti-tetrachiral [60]	Poisson's ratio –1. Isotropic anti-tetrachiral lattices have a transverse shear modulus that is similar to that of three-ligament configurations and, on average, 50% lower than that of hexachiral configurations.
Tetrachiral [58]	In-plane Poisson's ratio is −1. In contrast to the majority of other negative Poisson's ratio materials, the Poisson's ratio of their system is maintained throughout a wide range of strain.

In conclusion, the study of auxetic materials has revealed a vast array of structures and their unique properties. Among these, chiral, re-entrant, and rotating polygon structures have shown great promise in a range of applications. Chiral auxetics, in particular, have received increasing attention due to their potential for high stretchability and shape-morphing behaviour. The ability to control chirality and tune the mechanical properties of chiral structures offers exciting possibilities for designing new materials with specific functionalities.

2.1. Summary of Analysis of Structures Exhibiting a Negative Poisson's Ratio

Re-entrant structures, such as the double arrowhead, have shown promise in applications where deformation needs to be minimized. While complex to manufacture, advances in additive manufacturing techniques are making these structures increasingly viable for use in a range of applications. Rotating polygon structures, such as the hexagonal re-entrant model, have also shown promise in energy absorption applications. Their unique mechanical behaviour, which includes a negative Poisson's ratio and high energy absorption capacity, makes them ideal for use in crash protection and other impact-resistant applications. Overall, the study of auxetic materials and their unique properties has opened new possibilities for the design of materials with tailored functionalities. As a result of this study, the hexagonal re-entrant model will be further investigated for future experiments due to its promising properties in energy absorption.

3. Testing of Investigated Structures

3.1. Design of the Unit Cell

An auxetic re-entrant structure and a standard honeycomb structure were chosen to be investigated, firstly under a finite element analysis test, later compression tests were performed on 3D printed specimens. Printing was done with an FDM 3D printer using polylactic acid (PLA), which is the most commonly used biodegradable 3D printing material [61]. Since PLA is made from renewable resources like sugarcane or maize starch, it is a sound sustainable choice for experimental material. Compared to non-biodegradable plastics such as ABS, it is biodegradable, or capable of being broken down by natural processes, which lessens its environmental effect. As a sizeable portion of research for auxetic materials is made for medical purposes it is important to highlight PLA's biocompatibility, which means that it performs well when in contact with live tissues and does not have any negative side effects. This quality qualifies it for application in tissue engineering scaffolds, sutures and implants. PLA's main properties include [62]:

- Elastic Modulus (E): PLA has a relatively low elastic modulus, typically ranging from 2 to 5 GPa (2.34 GPa was chosen). This means that PLA is relatively flexible and has low stiffness compared to materials like metals. However, the exact elastic modulus of PLA can vary depending on the specific grade, processing conditions, and temperature.
- Poisson's Ratio (ν): PLA typically has a Poisson's ratio of around 0.35, which means that it has a moderate tendency to deform laterally when subjected to axial loading. Poisson's ratio measures the ratio of lateral strain to axial strain in a material when it is deformed under load.
- Density: The density of PLA is typically around 1.24 g/cm³, which makes it relatively lightweight compared to other materials used in AM. The low density of PLA can be advantageous in weight-sensitive applications.
- Tensile Strength: PLA has a relatively high tensile strength for a biodegradable polymer, typically ranging from 30 to 60 MPa – 49.5 MPa was chosen. Tensile strength measures the maximum amount of stress a material can withstand before it starts to deform plastically or fracture.

A modified (rotated) version of the standard auxetic cell [63] was chosen as the key area of further research. The typical hexagonal re-entrant cell is made up of six beams or struts that are organized in a closed-loop hexagonal design. A continuous network is formed by the connections between each beam and its neighbouring beams. The inward or concave curve of the beams at some spots, which gives it the re-entrant attribute, is the distinguishing feature of the hexagonal re-entrant cell. The geometrical layout of a standard re-entrant auxetic and hexagonal unit cells are depicted in Fig. 15.
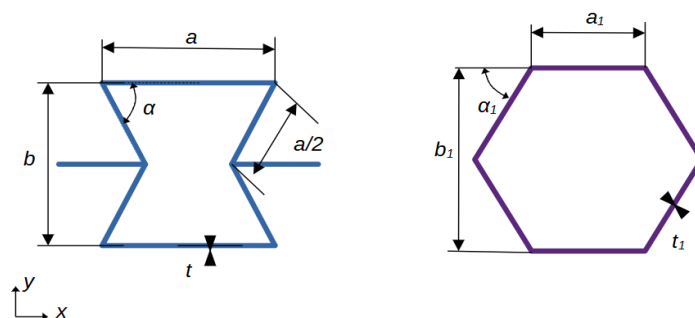
Fig. 15. Re-entrant and hexagonal unit cells

The following main geometrical attributes for the unit cells are indicated: the thickness of the structure's walls is t, length of walls (height) in y direction – b, in x direction – a in millimetres. The angle between the diagonal wall and direction x is depicted as α. Similarly, the hexagonal unit cell's parameters are attributed as the following: t_1, height of the unit cell – b_1, length of all walls – a_1 in millimetres. The angle between the diagonal wall and x axis is depicted as α_1. Since the hexagonal unit cell is depicted as equilateral and equiangular, all its sides are the same length, internal angles between walls are equal to 120°, making α_1 being equal to 60°.

By increasing the thickness of the cell walls t and t_1 in both the honeycomb and auxetic structures, the relative density of the cells can be increased. This increase in thickness makes the cell walls more resistant to bending and collapsing, resulting in a higher modulus and plateau stress. Additionally, the increased thickness of the cell walls causes them to come into contact with each other sooner, reducing the strain at which densification occurs.

The fundamental physical characteristic of relative mass density, commonly referred to as specific mass density or simply density, measures the mass of a substance per unit volume. It is a measurement of the amount of mass inside of a specific area . In materials science and engineering, relative mass density is a crucial attribute since it sheds light on how dense and heavy a substance is. It is frequently used to compare the densities of various materials or to determine whether a substance is appropriate for a given purpose. When utilizing porous structures for buildings and components in engineering, knowing relative density is essential where weight and strength are taken into account. Relative density of a re-entrant cell is presented in Eq. 1 :

$$\frac{\rho_u}{\rho_b} = \frac{\frac{2t}{a}(\frac{2a}{a}+2)}{2\cos(90-\alpha)(\frac{2a}{a}+\sin(90-\alpha))} = \frac{\frac{8t}{a}}{2\sin(a)(2+\cos(\alpha))} = \frac{8t}{a2\sin(a)(2+\cos(\alpha))}, \tag{1}$$

where: ρ_u is the density for the unit cell (g/cm³); ρ_b is the density for the bulk material (g/cm³); t is the thickness of the walls (mm); α is the angle of the diagonal wall (degrees); b is the length of the unit's vertical wall (mm); a is the length of the unit's diagonal wall (mm).

When a material is exposed to an applied force or stress, the Poisson's ratio, which is a property of the material, specifies the ratio of transverse strain (lateral deformation) to longitudinal strain (axial deformation). An analytical expression has been derived and verified for Poisson's ratio of honeycomb structures under uniaxial loading [64]. The deflection of honeycomb beams is assumed to behave similar to simple Euler beams. The equation for Poisson's ratio of regular honeycomb structures when loaded in the y direction, is presented in Eq. 2 . This equation can also be used for re-entrant auxetic unit cells by changing the angle θ to a negative value:

$$v_{yx} = -\frac{\epsilon_x}{\epsilon_y} = \frac{\sin^2(\alpha)}{\left(\frac{2a}{a}+\cos\alpha\right)\cos\alpha} = \frac{\sin^2(\alpha)}{(2+\cos\alpha)\cos\alpha}, \tag{2}$$

The relative density and Poisson's ratio of the unit cells were calculated using the Eq. 1 and Eq. 2 derived as shown in Table 3.

Table 3. Geometrical parameters for unit shapes

Unit shape	a, mm	t, mm	α (°)	ρ^u/ρ^b	v_{yx}
Auxetic1	6	0.45	60	0.115	-0.33
Auxetic2	6	0.90	60	0.231	-0.33
Auxetic3	6	1.35	60	0.346	-0.33
Auxetic4	6	1.80	60	0.462	-0.33
Auxetic5	6	2.25	60	0.577	-0.33
Hexagonal1	3	0.45	60	0.173	1.67
Hexagonal2	3	0.90	60	0.346	1.67
Hexagonal3	3	1.35	60	0.520	1.67
Hexagonal4	3	1.80	60	0.693	1.67
Hexagonal5	3	2.25	60	0.866	1.67

As learned from theoretical sources the gained poisons ratio for auxetic unit cells was achieved to be negative – -0.33 and positive for hexagonal units – 1.67. For auxetic structures, increasing the thickness of the walls by 0.45 mm yields an increase of relative density by 0.115 with each iteration. Analogically, for hexagonal cells it increases it by 0.173. This means that the same increase of wall thickness of 0.45 mm for hexagonal units, increases its relative density ~150% more than to an auxetic structure, thus making the latter one more space efficient.

3.2. Finite Element Analysis for Grid Structures

Main finite element analysis steps using Solidworks software:
  – Geometrical Data of unit cells was considered when making grid arrays of models of non-auxetic and auxetic structures.
  – Mesh was generated: geometry of models was divided into smaller, finite-sized elements.
  – Main material qualities were input into a custom material tab. Solidworks does not have data about PLA's properties by default.
  – Boundary conditions were applied to models.
  – FEA model under non-linear analysis was solved
  – Results of strain and stress were gained and compared.

The finite element structures were made using the unit cells discussed previously arranged into a five width by three height grid-like pattern, based on previously done research and recommendations [65, 66]. Firstly, the single inner unit cell is drawn with appropriate dimensions, as shown in Fig. 16, after which it is replicated in an array, with the cells being spaced from one another according to the thickness (preliminary default value taken as 0.45 mm). The five by three pattern allowed an adequate balance between intricacy and processing efficiency. The analysis requires less processing power since it is simpler than more complex grid layouts. However, it is also sufficiently intricate to describe the fundamental behaviour of auxetic and hexagonal models under compression. It also allows for comparison with other similarly done experiments.
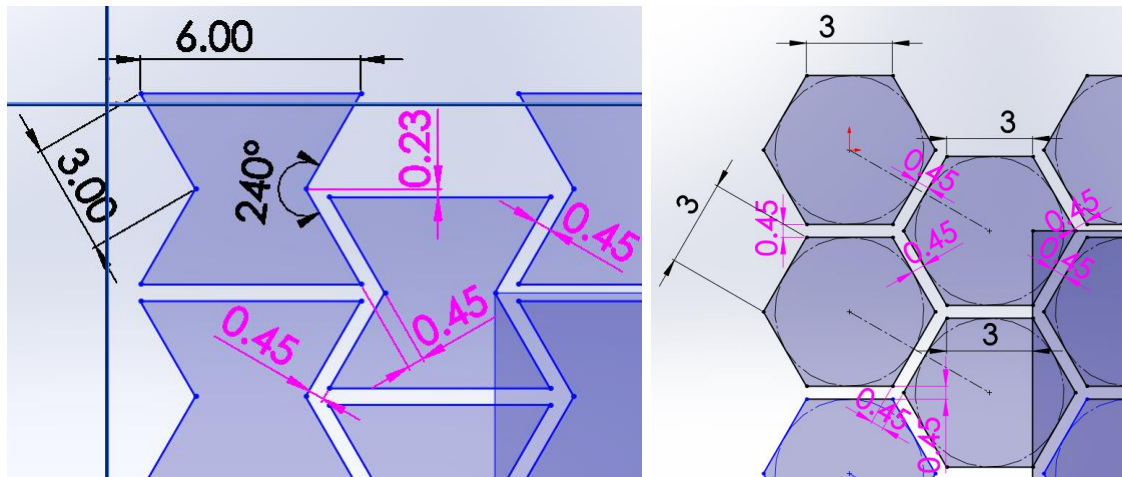
Fig. 16. Sketch of a an auxetic pattern (left) and hexagonal (right)

Then a bounding box is drawn to indicate an array of 5x3 to be extruded by 20 mm, examples of final shapes are shown in Fig. 17. Since the thickness is the only geometrical variable for both structures, the relevant thickness dimensions are selected and into a configuration design table to create structures with varied thicknesses. Nominal sizes of the models were altered accordingly to suit the geometrical restrictions of further done physical compression tests. Proper height, width and extrusion was needed to ensure an adequate surface area of horizontal plates which came into contact with the compression machine. Unfortunately, following international standardized compression parameters for plastics such as ISO 604 [67] or ISO 844 could not be followed, as they are meant for non-porous plastics, restrict geometrical parameters and are not suitable for 2D extruded structural models.
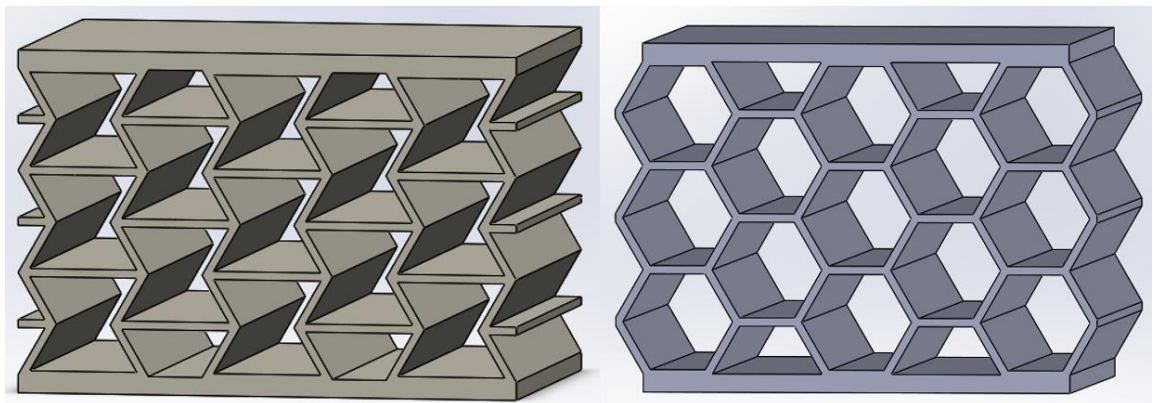
Fig. 17. Extruded 3D models of an auxetic (left) and hexagonal (right) structures

For the purposes of the compression test top and bottom plates of a height of 1 mm each were added to make the surfaces which would be compressed flat and relatively similar. The effect of increasing thickness to the grids, has resulted in the models being of varied height and width, consequently when applying compressive loads, different surface area upon forces is acting should be considered. In total five models for each structure were considered with the thickness varying from 0.45 to 2.25 mm. The total height and width of the samples were measured and inserted into Table 4, with the area being the result of the multiplication of width by the depth.

Table 4. List of samples for compression test

Sample name	t, mm	Height, mm	Width, mm	Area, mm²
A1	0.45	18.94	27.9	528.43
A2	0.90	20.29	31.79	645.02
A3	1.35	21.64	35.69	772.33
A4	1.80	22.99	39.59	910.17
A5	2.25	24.34	43.49	1058.55
H1	0.45	18.94	23.34	442.06
H2	0.90	20.29	25.68	521.05
H3	1.35	21.64	28.01	606.14
H4	1.80	22.99	30.35	697.75
H5	2.25	24.34	32.69	795.67

Finite element analysis was applied by using, blended curvature-based meshes for the models with the following chosen parameters: element size – 2 mm, element size growth ratio – 1.4, quality set to high with 16 Jacobian points. Since Solidworks does not possess material properties of PLA, the values for elastic modulus, density, tensile strength and Poisson's ratio were manually inserted:

- Elastic modulus 2.346 GPa
- Poisson's ratio 0.35
- Shear modulus 10.92 MPa
- Mass density 1240 kg/m^3
- Tensile strength 49.5 MPa

The created material properties were then applied to the extruded models. Fixtures were applied to the bottom plates, with all degrees of freedom being fixed. To simulate the upcoming physical compression test, a nonlinear static study was performed. Due to the nature of the actual compression's machine behaviour to operate in terms of a fixed compression rate and no actual input of force applied, the external load for the simulation was expressed as a displacement of 2 mm/min of the top plate was applied to structure. The meshed models are shown in Fig. 18, where fixtures are denoted in red arrows, applied displacement – blue arrows.
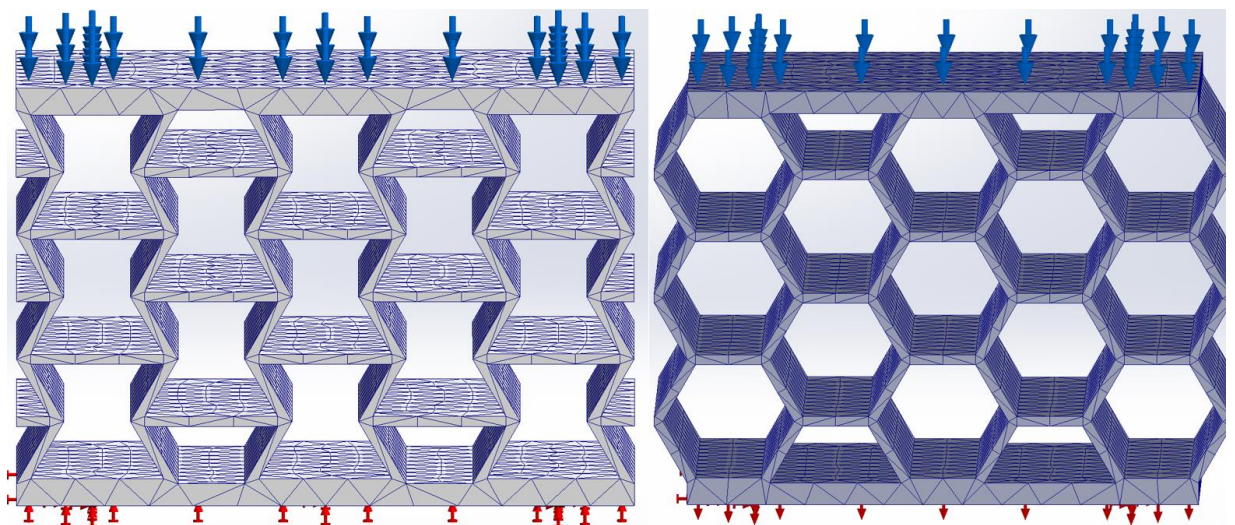
Fig. 18. Loads applied to auxetic and hexagonal structures
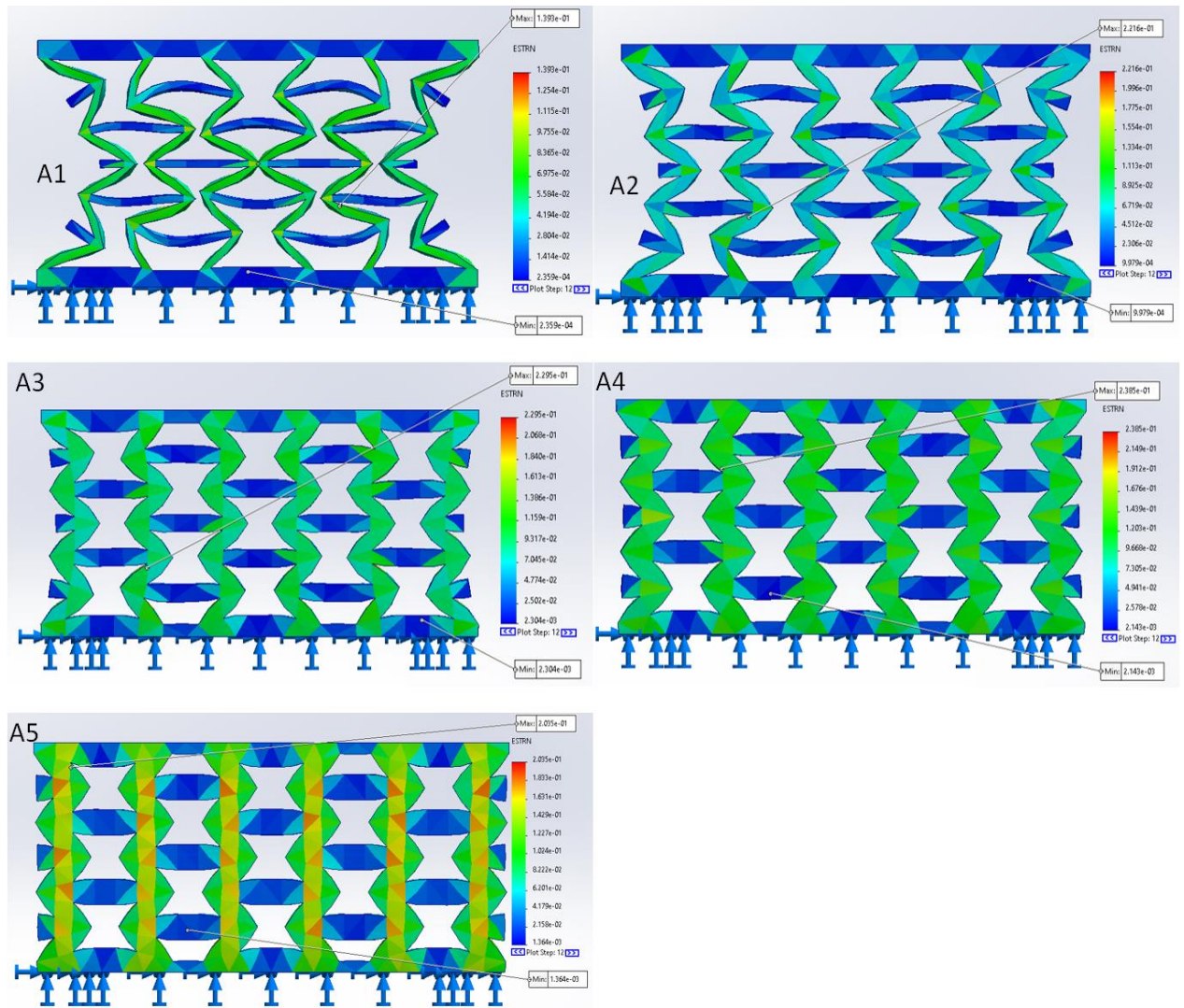
Fig. 19. Strain results for auxetic models

Strain results were gained, shown in Fig. 19 and Table 5, to indicate the deformation of a material in response to the applied compressive displacement. It is defined as the ratio of the change in deformation of a material to its original length. In other words, the resulting strain values indicate the amount of deformation per unit length. When comparing each model's results, a tendency for the maximum strain values was observed to increase for structure A1 to A4 – 1.393×10^{-1}, 2.216×10^{-1}, 2.295×10^{-1} and 2.385×10^{-1}. This could mean that the structure is becoming more compliant and deformable as thickness increases. This is because the thicker walls allow for greater deformation under compression, which results in a higher strain. However, a decrease in maximum strain was observed in the thickest model A5 – 2.035×10^{-1}, which would indicate its higher resistance to deformability.

Table 5. Minimum and maximum strain values for auxetic model's simulation

Model	Minimum Strain	Maximum Strain
A1	2.359×10^{-4}	1.393×10^{-1}
A2	9.979×10^{-4}	2.216×10^{-1}
A3	2.304×10^{-3}	2.295×10^{-1}
A4	2.143×10^{-3}	2.385×10^{-1}
A5	1.364×10^{-3}	2.035×10^{-1}
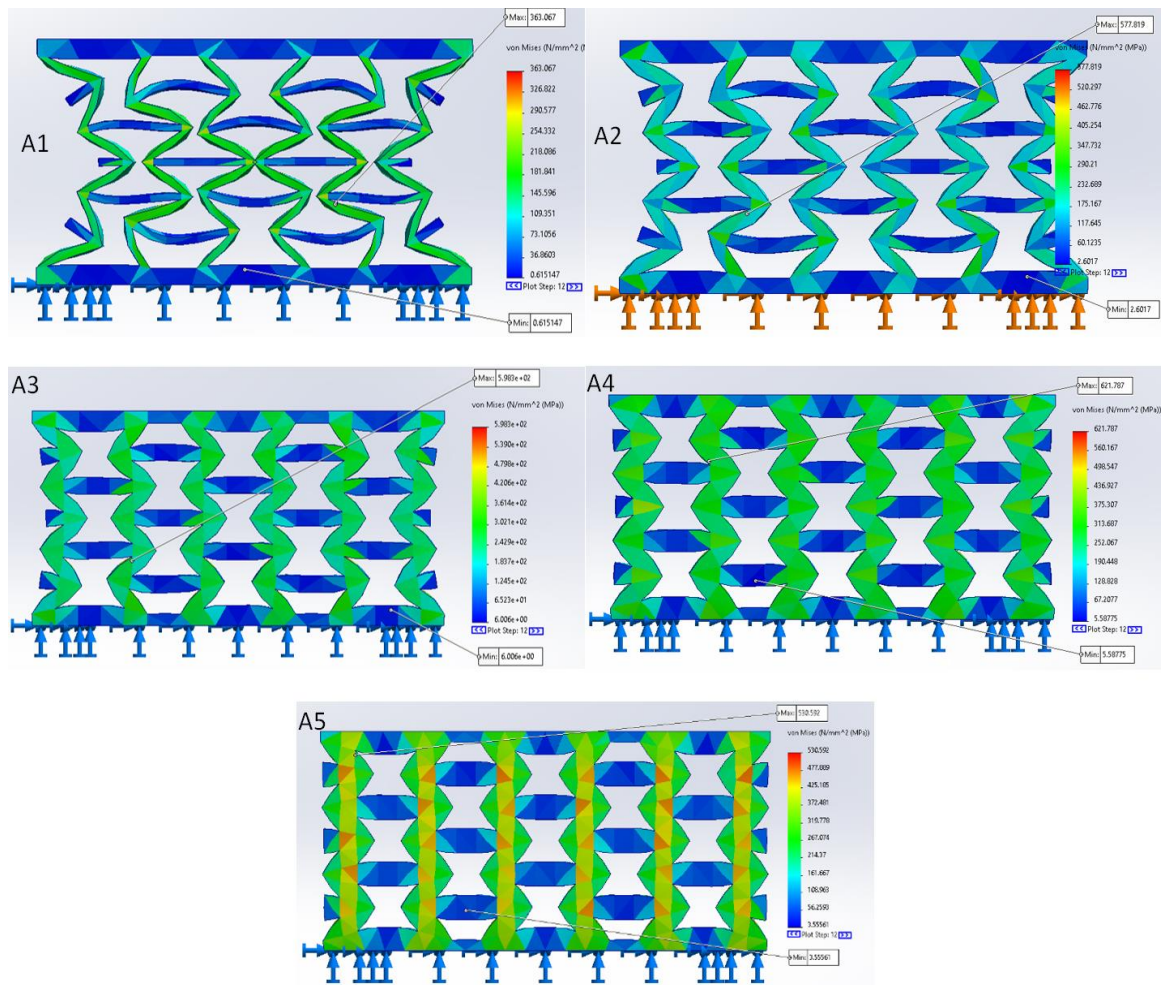
Fig. 20. Stress results for auxetic models

Simulated stress results from Solidworks shown in Fig. 20 and Table 6, indicate the distribution and magnitudes of stresses within the models A1–A5, as well as maximum values of the models: 363.067 MPa, , 577.819 MPa, 598.3 MPa, 621.787 MPa and 530.592 MPa. As can be indicated by the numbers, the maximum stress tends to increase with each iteration, except for the fifth one. This is analogous to the strain results and could indicate the following parameters upon the fifth model: inadequate meshing quality, uncompliant geometrical parameters for the study. The results are from internal forces that develop within a material in response to external loads and is represented by a vector quantity that describes the amount and direction of force at each point in the material. As indicated in theoretical findings, the auxetic models are shown to contract in lateral directions when compressed. When an auxetic structure is compressed, it typically turns inwards due to this negative Poisson's ratio effect. This effect is visibly discerned in A1 and A2 models, with A3, A4, A5 models showing little deformation due to increased wall thicknesses.

Table 6. Minimum and maximum stress values of auxetic model's simulation

| Model	Minimum Stress, MPa	Maximum Stress, MPa
H1	0.615	363.067
H2	2.602	577.819
H3	6.006	598.3
H4	5.588	621.787
H5	3.556	530.592
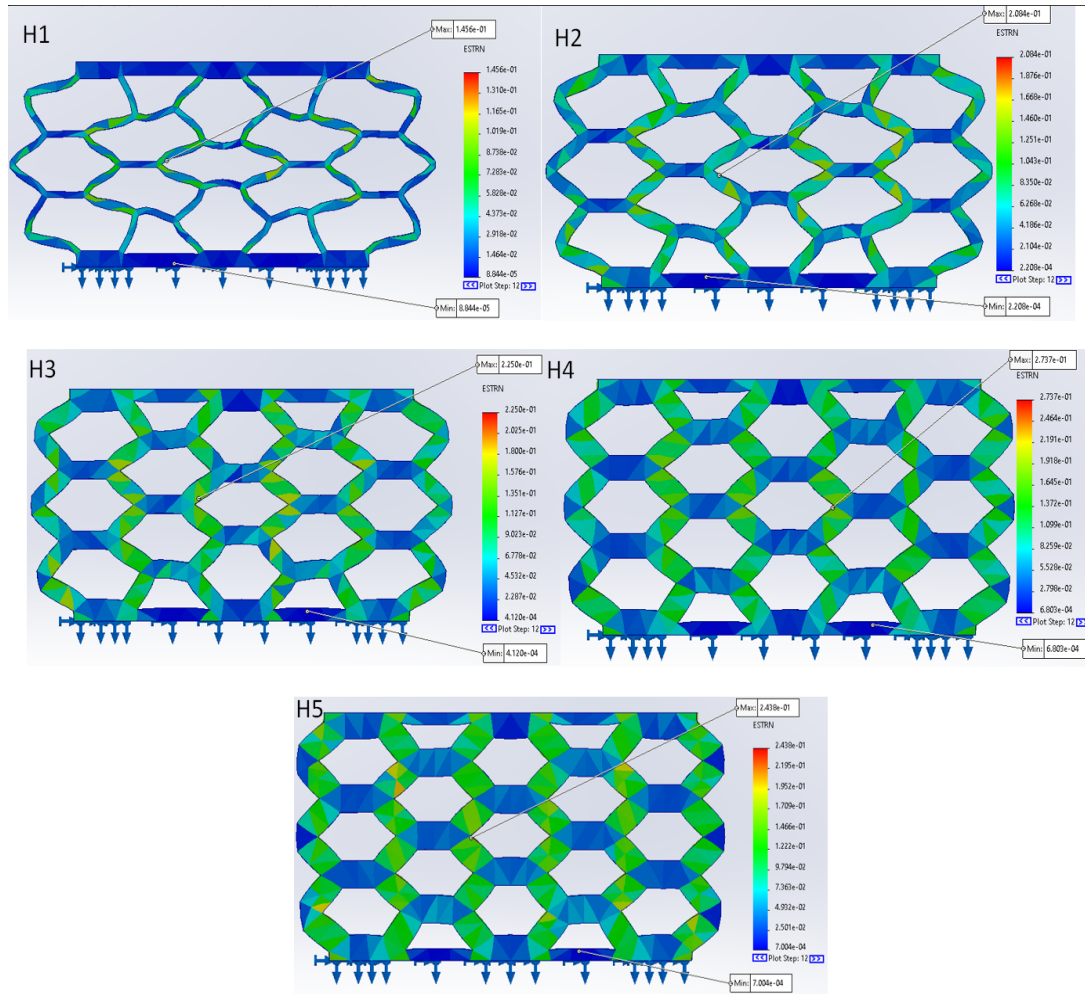
Fig. 21. Strain results for hexagonal models

Simulated strain results from Solidworks shown in Fig. 21 and Table 7, indicate the distribution and magnitudes of stresses within the models H1–H5, with the following maximum values: 1.456×10^{-1}, 2.084×10^{-1}, 2.250×10^{-1}, 2.737×10^{-1} and 2.438×10^{-1}. The numbers indicated that strain increased as thickness of walls was increased, omitting the fifth iteration, since it displayed a lower maximum strain than the fourth iteration. The results are from internal forces that develop within a material in response to external loads and is represented by a vector quantity that describes the amount and direction of force at each point in the material. As indicated in theoretical findings, the hexagonal models are shown to expand in lateral directions when compressed. This effect is visibly discerned in H1 and H2 models, with H3, H4, H5 models showing little deformation due to increased wall thicknesses.

Table 7. Minimum and maximum strain values of hexagonal model's simulation

Model	Minimum Strain	Maximum Strain
H1	8.844×10^{-5}	1.456×10^{-1}
H2	2.208×10^{-4}	2.084×10^{-1}
H3	4.120×10^{-4}	2.250×10^{-1}
H4	6.803×10^{-4}	2.737×10^{-1}
H5	7.004×10^{-4}	2.438×10^{-1}
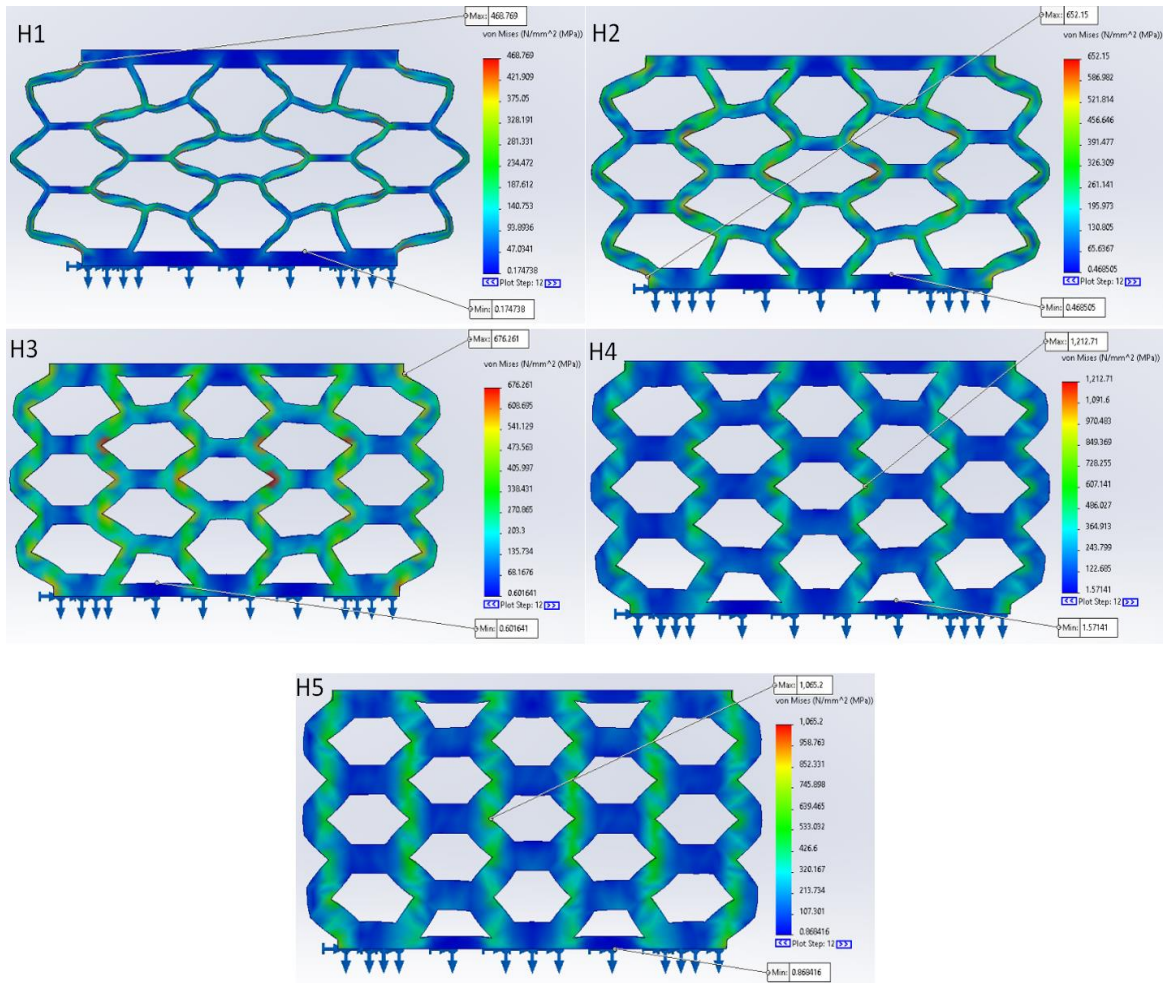
Fig. 22. Stress results for hexagonal models

Stress models in SolidWorks simulation can show which areas of the hexagonal structure are under the most stress, shown in Fig. 22 and Table 8, and may be susceptible to failure. This can inform the design of the structure to reinforce those areas or to reduce the stress concentration. Additionally, simulation can predict how the hexagonal structure will deform under different levels of compression, allowing for the optimization of the geometry for maximum energy absorption or minimum deformation. The maximum stress values for models H1 to H5 were: 468.769 MPa, , 652.15 MPa, 676.261 MPa, 1212.71 MPa and 1065.2 MPa. These numbers similarly to previous simulation results indicate a trend between the first four iterations – an increase in stress each time, but the fifth model shows unique behaviour. Overall, since all models had same fixtures, loads and meshes applied to them, it could indicate gaps in the simulations, such as an unoptimized mesh element type, mesh density and convergence criteria.

Table 8. Minimum and maximum stress values of hexagonal model's simulation

Model	Minimum Stress, MPa	Maximum Stress, MPa
H1	0.174	468.769
H2	0.469	652.15
H3	0.602	676.261
H4	1.571	1212.71
H5	0.868	1065.2

34

3.3. 3D Printing of Structures

Experimental work steps were made in the following order:

- PrusaSlicer software was used to project printing of all specimens, by converting and importing previously modelled structures as *.stl* files.
- Printing positions were set on the largest surface areas.
- Optimal printing settings were pursued, considering the following conditions: layer thickness, infill percentage.
- Each structure was printed using a fused deposition modelling 3D printer.

After inserting the .stl models into PrusaSlicer software, as indicated in Fig. 23, additional parameters for optimal printing were considered. The orientation of the parts can have a significant impact on the printing time and quality. Parts were oriented so that they have the fewest overhangs and support structures possible. This will minimize the amount of material needed for supports and reduce printing time. The parts were set to print on the largest surface areas. Similar structures were grouped together, which allowed to apply the same settings to multiple parts at once, which can save time and reduce the risk of errors.
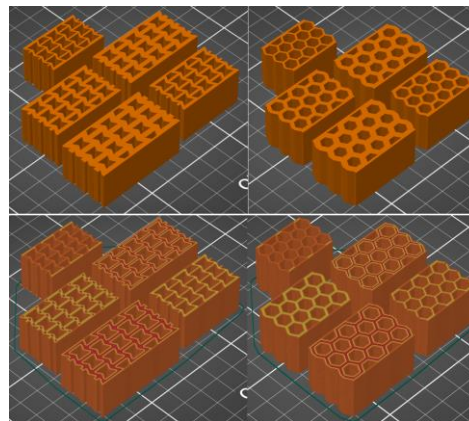
Fig. 23. Imported parts in PrusaSlicer, with sliced previews

Corresponding to geometrical parameters, such as surface area, height and width, printing path complexity the auxetic structures were shown to have a total print time of 15 hours and 46 minutes and a 68.37 g of filament, while hexagonal models printing time was 10h 3min and 49.03g of filament was used, indicated in Fig. 24.

Fig. 24. Printing times and filament used for model groups: a) auxetic, b) hexagonal

Both models were printed using the same printing parameters of 0.15 mm layer height, first layer height – 0.2 mm, infill density – 100%, fill pattern – rectilinear, non-print travel speed – 180 mm/s, print move speeds ranging from 25 to 80 mm/s.

A Prusa i3 MK3S+ 3D printer was used to produce the required parts. The filament, shown in Fig. 25, was loaded into the printer by inserting it into the filament sensor and feeding it through the extruder. The extruder was then calibrated by using the built-in firmware calibration routine. This ensured that the printer was accurately extruding the filament.

Fig. 25. Original Prusa i3 MK3S+ 3D printer [68] and filament [69]

The following technical parameters for the Prusa i3 MK3S+ 3D printer were acquired [68]:

Table 9. Original Prusa i3 MK3S+ 3D printer parameters

Parameter	Description
Build Volume	25×21×21 cm
Layer height	0.05 - 0.35 mm
Nozzle	0.4 mm default, wide range of other diameters/nozzles supported
Filament diameter	1.75 mm
Max travel speed	200+ mm/s
Print surface	Removable magnetic steel sheets (*) with different surface finishes, heat bed with cold corners compensation
Printer dimensions (without spool)	7 kg, 500×550×400 mm (X×Y×Z)
Power consumption	PLA settings: 80 W

The printed samples, Fig. 26, were checked for their nominal dimensions and especially wall thicknesses for deviations from CAD models.

Fig. 26. Printed samples marked as A1-A5 – auxetic; H1-H5 – hexagonal

3.4.   Compression Tests of Printed Samples

For the compression tests for the models a Tinius Olsen H25KT testing machine was used, shown in Fig. 27.

Fig. 27. Tinius Olsen H25KT testing machine

The Tinius Olsen H25KT machine has the following technical parameters to be utilized [70]:

– Load measurement accuracy: +/- 0.5 % of indicated load from 2 % to 100 % capacity.
– Extended range down to 1 % capacity with accuracy of 1% of indicated load.
– Position measurement accuracy: +/- 0.01 % of reading or 0.001 mm.
– Speed accuracy: +/- 0.005 % of set speed.
– Power: standard optional voltages 220/240 VAC, 50-60 Hz, 2000 W.

The steps taken for testing the samples:

– The compression machine was prepared: parameters, such as the compression speed (2 mm/min), load cell capacity (25 kN), and test duration (4 min) were bound.
– Sample was installed: sample was placed on the lower compression plate and aligned so that it is centred and level. The upper compression plate was then lowered using the software interface until it came into contact with the sample.
– Load and displacement were zeroed: the machine 's interface was used to set the load and displacement values to zero, to ensure accuracy of the load measurements.
– Test was conducted: compression machine was started and let to run until the desired compression distance was reached.
– Sample was removed: Once the test was complete for a sample, the machine was stopped, the upper plate was heightened, sample was removed, and another one was placed. Steps 2 to 5 were repeated for each part.
– Data and graphs of resulting forces versus displacement were gained and plotted from the machine's software. The data points were recorded with extension increments of 0.0125 mm.

As was discussed in theoretical sources, the auxetic structure eventually collapses within itself, shown in Fig. 28., meaning a decrease in height and a decrease in width when acted by compression. As compression increases, the struts within the grid increase in length, causing the cells to deform and rotate, which makes the entire system contract transversely.
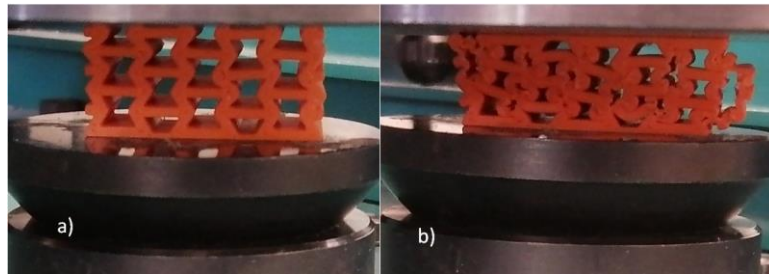
Fig. 28. Comparison of A3 structure at: a) start of compression, b) end of compression

During the test, the hexagonal cells indicated slight shear deformation, as majorly only upper cells within the system underwent deformation during initial testing time. Eventually, all cells were subjugated to the loads, which resulted in the hexagon models acting more uniformly. Towards the later stages of compression, shown in Fig. 29, the hexagons became more circular in shape, causing the model to decrease in height and increase in width substantially when compared to the auxetic counterparts.
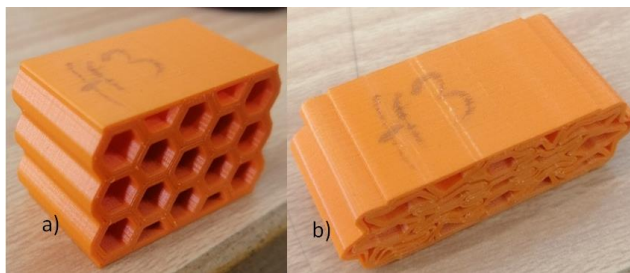
Fig. 29. Comparison of A3 structure at: a) start of compression, b) end of compression

Compressive behaviour of the models was also affected by the printing parameters. Since, the principal of an FDM printer is to extrude material through a limited diameter nozzle, latter iterations of samples were printed with a higher number of fused layers. During compression, the heterogeneity nature of the models caused the walls of the specimen to ultimately detach from one another and split into multiple parts. Effects of this can be seen in the ending phases of both structures. Contrastingly, reviewing a similar experiment performed on 3D printed samples [43], shown in Fig. 30 both hexagonal and auxetic models performed differently.
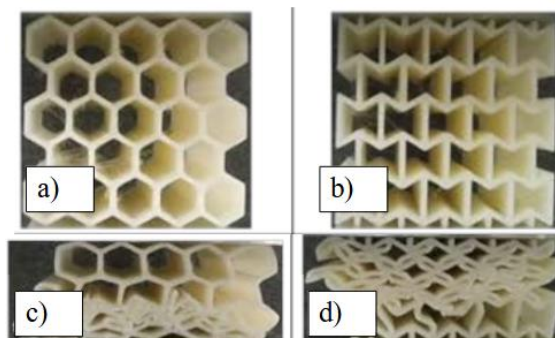
Fig. 30. Deformation modes: a) hexagonal start; b) hexagonal end; c) re-entrant start; d) re-entrant end [43].

During initial compression phases, the central to lower unit cells were the only ones affected. This can be explained by the choice to use external supporting plates instead of printed upper and lower plates for the models, causing the load to be applied less uniformly upon the contact points between machine and unit cells. On further comparison of experimental results, the unit cells also differ in rotation, however, both approaches yield expansion and contraction in width for auxetic and hexagonal models, respectively.

Comparatively, in another similar study experiments on FDM 3D printed was performed, shown in Fig. 31 [71]. The final observed compressed model highlighted visible skew behaviour of the layers. This could indicate shear failure, which happens when the material or adhesive between the layers is stretched beyond its shear strength. As a result, the layers may slide past one another, distorting and skewing the structure.
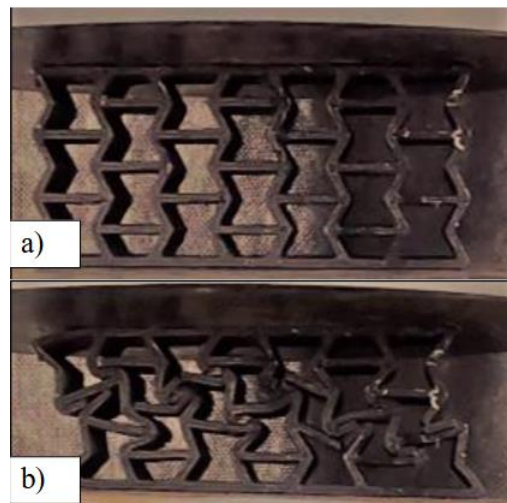
Fig. 31 Performance in a compression test: a) start; b) end [71]

Finally, a similar compression test was performed [42], shown in Fig. 32. The central links of the hexagonal honeycomb model have failed, while the rest of the cells persevered and conserved a relatively similar shape as it was modelled initially. The auxetic model behaved more uniformly, allowing all walls of the cells to withstand applied compression in unison.
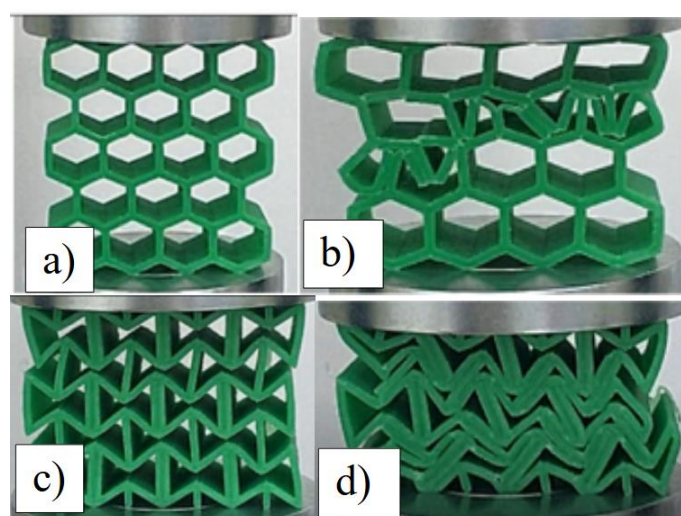
Fig. 32. Stages of experimental deformation: a) honeycomb start; b) honeycomb end; c) re-entrant start; d) re-entrant end [42]
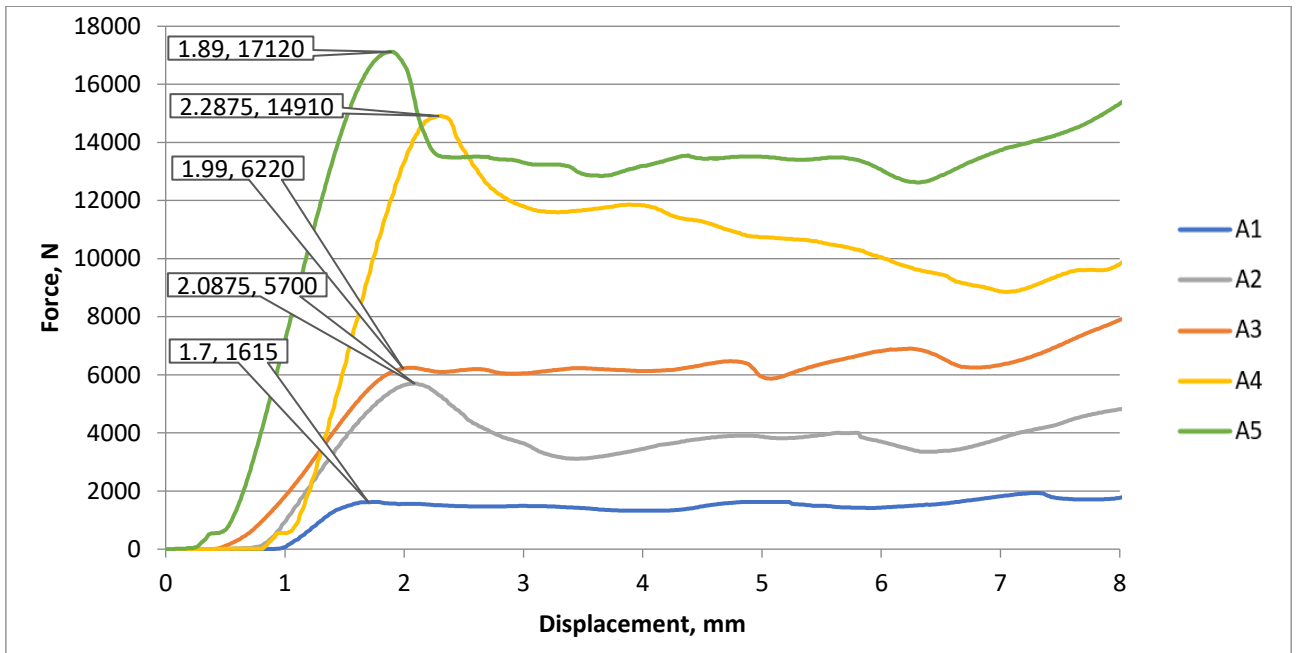
Fig. 33. Force versus displacement graph, auxetic structures
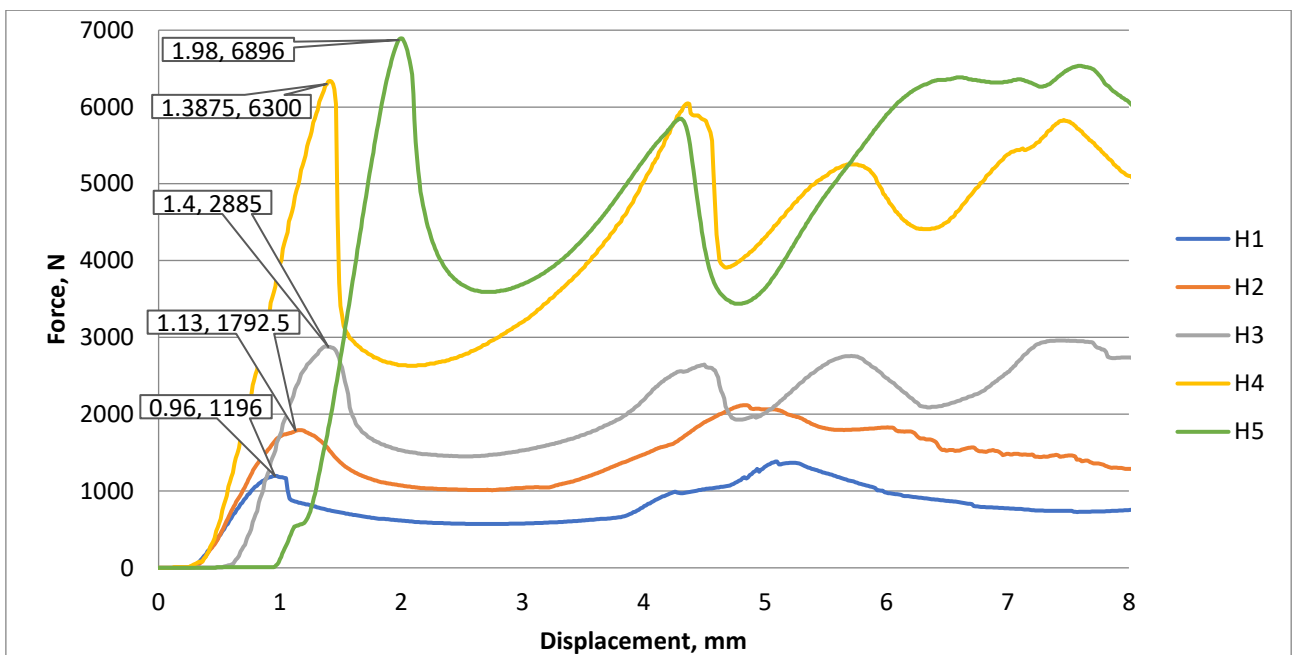
Fig. 34. Force versus displacement graph, hexagonal structures

The indicated graphs depict raw data gained from all compression tests upon the models, with first peak values marked, indicating the stiffness regions. Auxetic structures, contrary to hexagonal ones, after the first peak (maximum compression strength). Linking this to theoretical data, it can be extrapolated that the re-entrant model performs more uniformly, with inner reaction forces being relatively evenly distributed. The re-entrant approach also causes the structure to condense on itself when acted by compression, which prompts the structure at latter displacement points to deform into built-up densified areas, causing the grid to withstand higher compressive loads. From the first iteration and onwards, the re-entrant models indicate the capacity to withstand higher forces under the same displacement values when compared to their hexagonal counterparts. Results of both approaches indicate no significant drops in resulting forces and thus a tendency to perform as

homogenous structures after the 6 mm displacement point. Since thickness of walls become irrelevant in this aspect, the compressive test limits can be linked to the set initial geometrical parameters of fixed wall heights and the five-by-three grid layout.
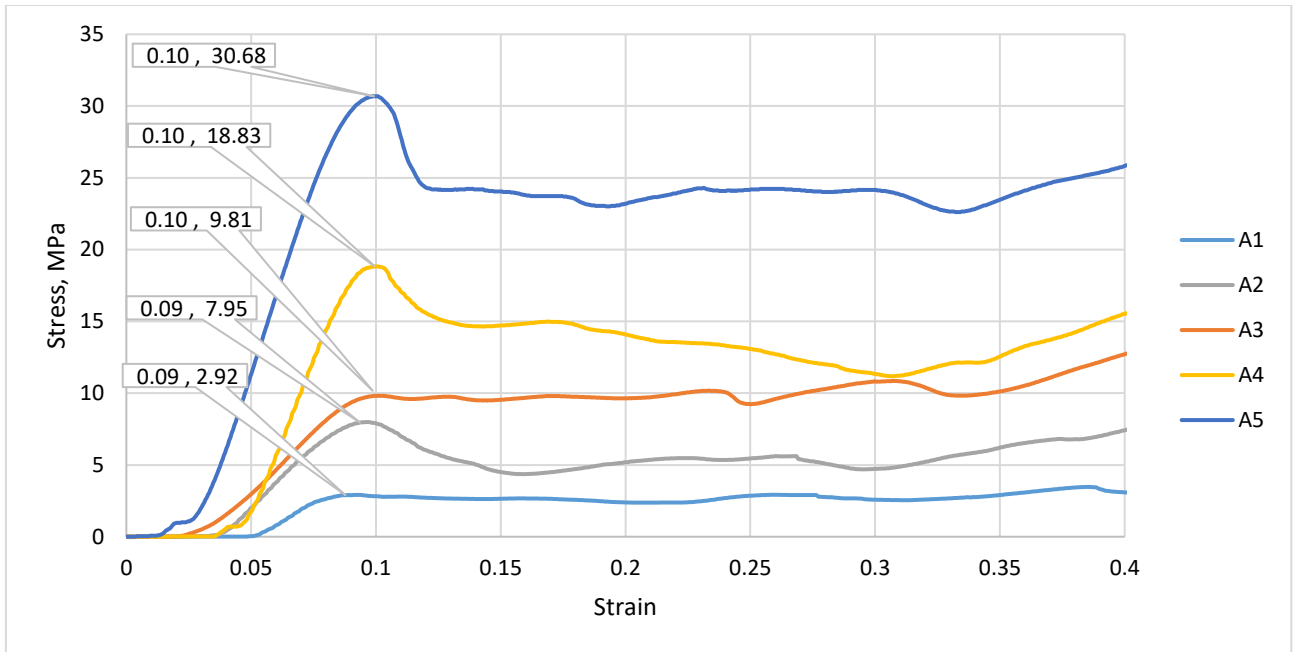
Fig. 35. Stress versus strain graph for auxetic samples
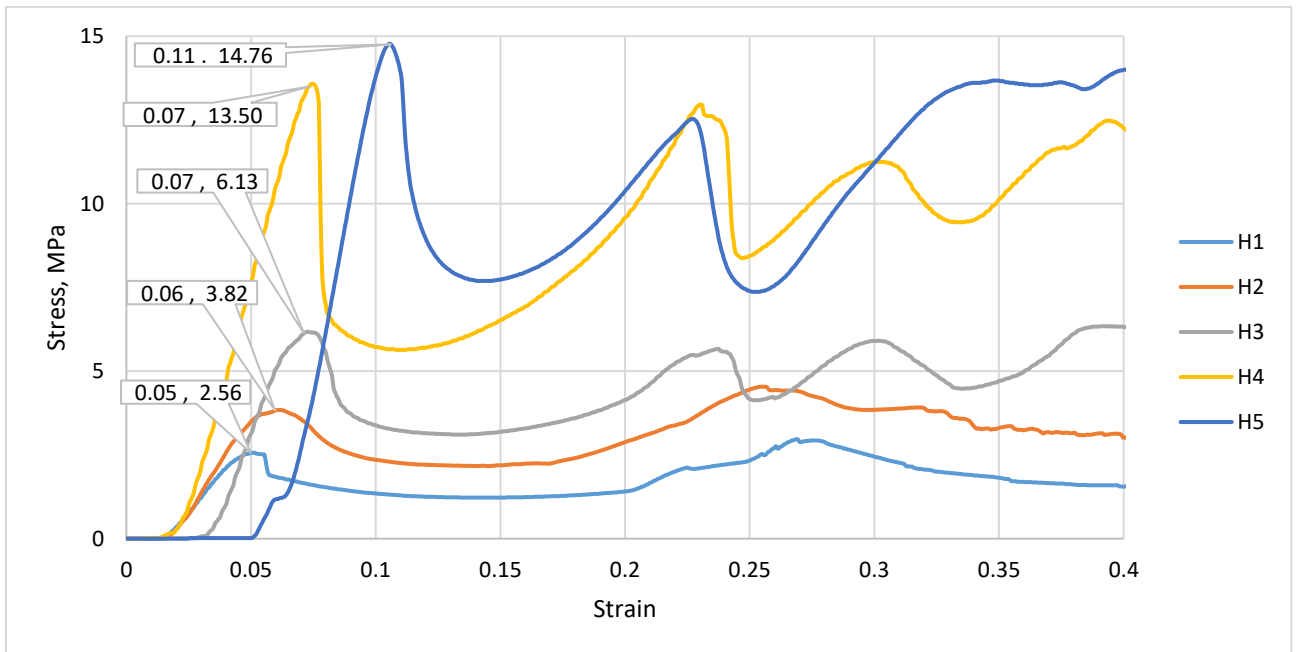
Fig. 36. Stress versus strain graph for hexagonal samples

Strain was calculated from the displacement versus force graph, by indicating change in displacement divided by the height of the specimen. Stresses were calculated by dividing resulting forces by surface areas under compression of each structure, resulting graphs were drawn. The auxetic models indicated an exponential sudden increase and then a constant value of stress. Meanwhile, as thickness for the hexagonal models increased, the amplitudes of stresses increased as well. When selecting a structure type for a model in further applications, it is important to discern the advantages. The auxetic re-

entrant specimens indicate a loss of, but still a relatively high and constant stress endurance after the initial maximal value. On the other hand, the hexagonal specimens indicate an increase in instability as thickness of unit cell walls increase, which would be beneficial if a heterogeneous material optimization approach were to be applied. By doing this, saving costs on non-affected and focusing more on the unit cells most affected by compression would stabilize the results. As a result, unnecessary material can be minimized, but more analysis needs to be done if this would be cost effective to a homogenous re-entrant model.

Young's Modulus for the models was found from the force versus displacement values and graph. It is depicted as the ratio of stress versus strain inside of the linear portion of the graph. For more accurate results the SLOPE function in excel was used. The force and displacement data were entered into two columns in Excel, with the independent variable in one column and the dependent variable in the other. The formula "=SLOPE(dependent variable range, independent variable range)" was used, by replacing "dependent variable range" and "independent variable range" with the range of cells in the data set. The result was the slope value of the linear regression line. This value was then divided by the cross-sectional area of each specimen. The values were then inserted into Fig. 37.
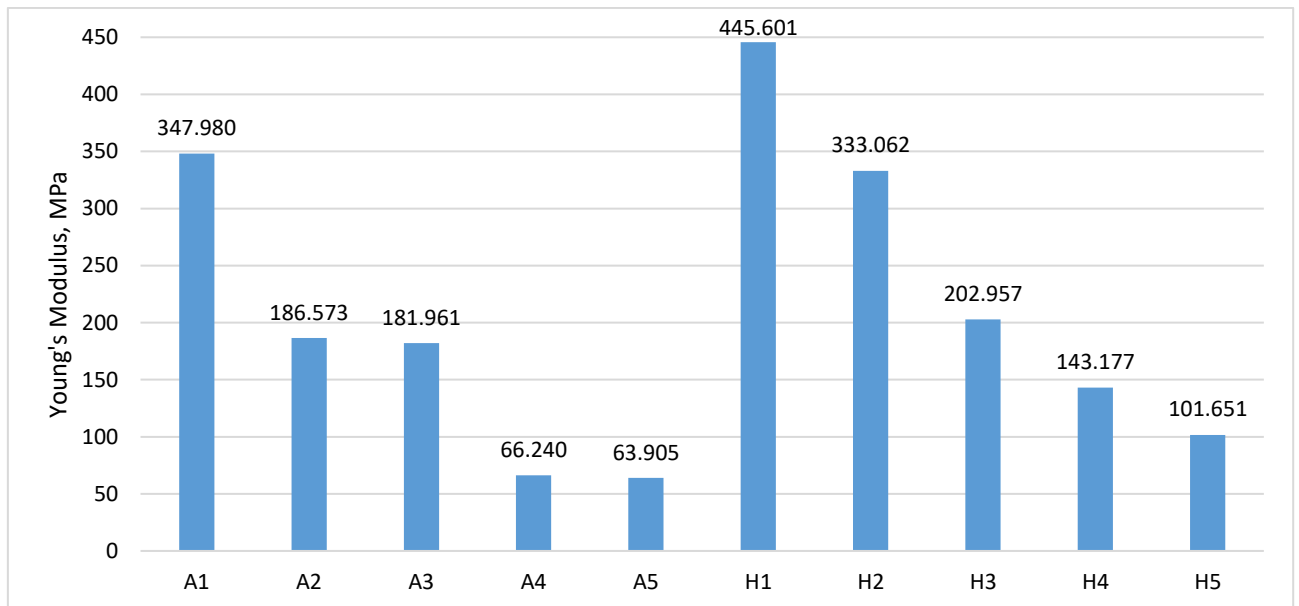
Fig. 37. Young's Modulus results

The quantity of energy wasted or absorbed by a material or system as a result of loads or external forces is referred to as absorbed energy [72]. It is a measurement of the energy conversion that takes place during deformation or impact inside the material or system. Energy is imparted to a material as it deforms, whether by compression, tension, bending, or any other kind of stress. Elastic potential energy and internal strain energy are two examples of the several ways that this energy can be kept in the material. The material experiences changes in form, volume, or structure as it absorbs external energy to adapt to the forces being applied. In context of applying this to novel material structures in real life scenarios it is an indicator for guaranteeing the functionality and safety of numerous systems and goods. The energy is often computed from the complete force-displacement curve rather than from a particular point in the case of energy absorption during a compression test. The amount of work done on the material throughout the course of the whole compression process is represented by the energy absorbed. Calculation of absorbed energy is performed using Eq. 3 [73]:

$$W = \int_0^\varepsilon \sigma(\varepsilon)d\varepsilon, \tag{3}$$

A measurement of the energy absorbed by a substance or structure per unit mass is known as specific energy absorbed, also known as specific absorbed energy or specific impact energy. In many different applications, including impact-resistant materials, crashworthiness study, and protective equipment, it is frequently used to assess the energy-absorbing capability of materials and structures. Specific energy absorbed is calculated using Eq. 4 [73]:

$$W = \frac{\int_0^\varepsilon \sigma(\varepsilon)d\varepsilon}{m}, \tag{4}$$

where: σ is the stress for the model (MPa); ε is the strain; m is the mass of a specimen (g). Mass of each specimen was measured using a scale.

Values for absorbed energy and specific absorbed energy were calculated and plotted into Fig. 38 and Fig. 39.
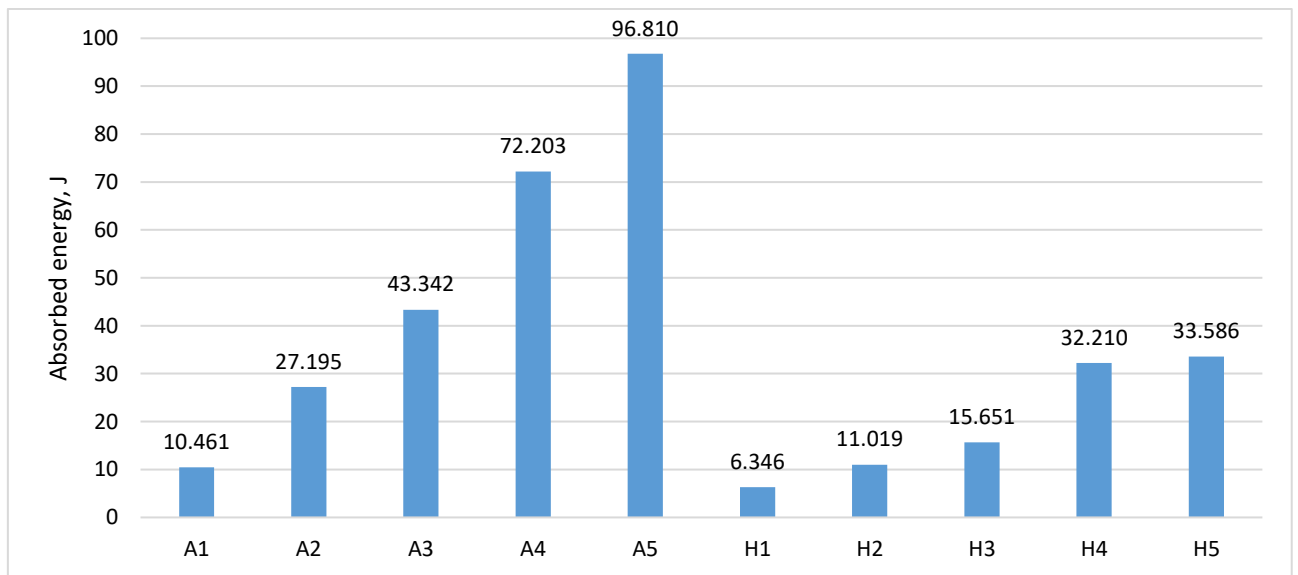
Fig. 38. Absorbed energy for each model
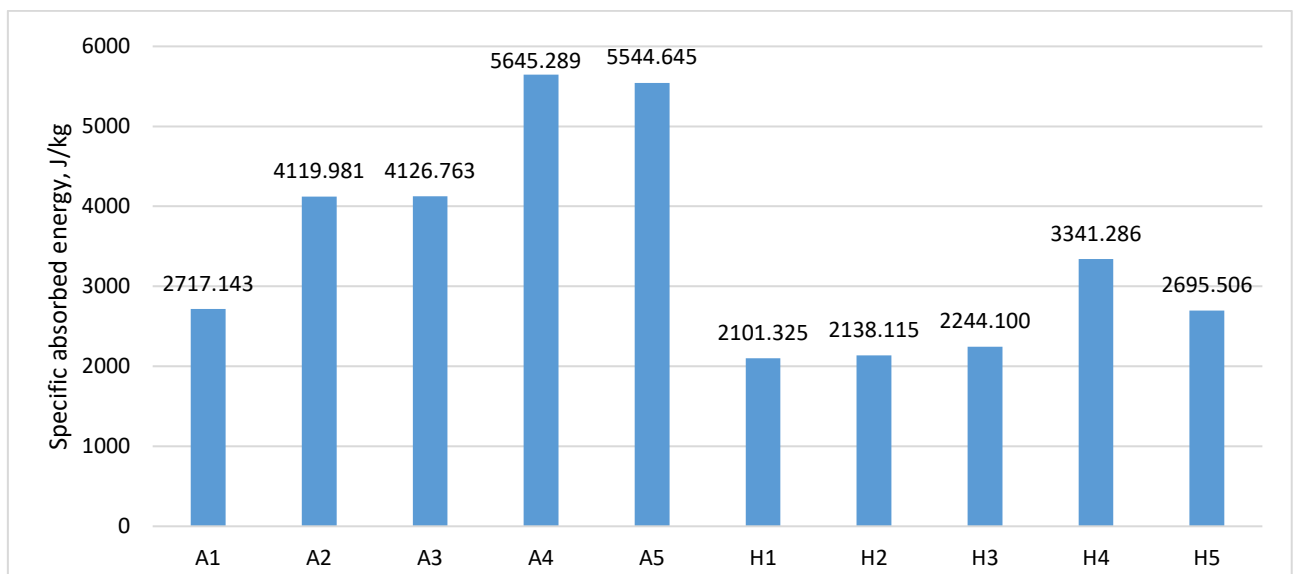
Fig. 39. Specific absorbed energy for each model

Judging from the former Fig. 38, absorbed energy tends to rise with the increase of wall thickness. It implies that with each iteration, structures get better at enduring and releasing energy from applied stress. This increase in energy absorption can have a number of effects and be seen favourably in a variety of situations. The ability of a material or structure to tolerate increased amounts of impact or stress without failing is primarily implied by a rising trend in specific energy absorption. For the auxetic models an exponential increase was observed with each iteration. On the other hand, the hexagonal specimens performed worse, showing a lower ability for the models to endure energy, despite the increase of wall thickness.

More informative conclusions can be drawn from the specific absorbed energy values since they are a ratio of total absorbed energy and mass of a model. The data indicates that specific absorbed energy tends to increase on the second and fourth iterations, while being stagnant for the third and fifth iterations. This could be a result of geometrical design and 3D printing parameter peculiarities, as models with every increase in wall thickness should increase in mass gradually in theory, but not necessarily indicate that in reality. The values for each iteration and the average value for the specific absorbed energy of auxetic models – 4430.764 J over that of the hexagonal models – 2504.066 J/kg indicate a lack of the structure to absorb energy, despite an increase in material used.

Comparing gained values with previous works, trends across the experiments were observed. In [43] re-entrant structures show a 239.49 % rise in compressive strength, a 147.44 % rise in Young's modulus, a 129.76 % rise in energy absorbed and a 4.59 % decrease in specific energy absorbed. Compression tests performed in this project indicated a 172.45 % rise in compressive strength, a 69.03 % decrease in Young's modulus, a 253.02 % rise in absorbed energy and a 176.94 % increase in specific absorbed energy. The decrease in Young's modulus indicated that the proposed auxetic structures indicate higher flexibility, impact absorption, damping capacity and stress concentration. Since averages of both structural groups were used for this comparison, the auxetic re-entrant models exhibit superior improvement over their hexagonal counterparts in mechanical capabilities than that seen in the previously discussed work [43].

3.5.   Summary of Testing of Investigated Structures

The chosen geometrical parameters for both unit cells provided a discernible comparison between both models with the applied variable of wall thicknesses. The objective of modelling and simulating five by three extruded grid layouts was completed. A tendency was observed of increased mechanical properties as strut thickness increased. Fifth iterations of both model groups showed divergent result from the trend, indicating flaws in the performed finite element analyses. Justifiably this was caused by lack of mesh optimization for all models.

The CAD models were altered and imported into the 3D printer software. Printing parameters for optimal further experimental results were considered, such as infill density, nozzle diameter, layer height. Printed models were produced without any noticeable defects. Compression tests were accomplished by displacing the upper compression plate onto the specimen with a fixed rate of 2 mm/min. Observed and calculated trends of mechanical properties for both groups indicated successfully performed tests.

The practical study conducted a comparison between auxetic and hexagonal structures in terms of their Young's modulus and compressive strength, when acted by compression. The results showed that the auxetic structures had lower Young's moduli than the hexagonal ones on average –169.332

MPa compared to 245.29 MPa, which indicated their ability to deform under pressure more easily. On the other hand, the compressive strength of the auxetic structures was higher than that of the hexagonal ones, on average 14.119 MPa compared to 8.187 MPa, which meant that they could withstand more force before failure. This difference in performance is due to the unique property of auxetic structures to expand in all directions when stretched and narrow when compressed, which allows them to distribute the stress more evenly throughout the structure. The lower Young's modulus of the auxetic structures may also make them more cost-effective than the hexagonal ones, as they require less material and energy to produce. Overall, the findings of this study, shown in Table 10 highlight the potential of auxetic structures as a promising alternative to traditional hexagonal structures in various engineering applications.

Table 10. Summary of experimental values gained from compression tests

Model	Young's modulus, MPa	Maximum stress, MPa	Absorbed energy, J	Specific absorbed energy, J/kg
A1	347.980	2.921	10.461	2717.143
A2	186.573	7.985	27.195	4126.763
A3	181.961	10.176	43.342	4119.981
A4	66.240	18.831	72.203	5645.289
A5	63.905	30.681	96.810	5544.645
H1	445.601	2.562	6.346	2101.325
H2	333.062	3.840	11.019	2244.1
H3	202.957	6.180	15.651	2138.115
H4	143.177	13.582	32.210	3341.286
H5	101.651	14.773	33.586	2695.506

4. Economic Benefits of Printing NPR Structures

To calculate cost effectiveness between the NPR and hexagonal 3D printed models, key variables should be taken into account. The printing time and required amount of filament for each model separately, was acquired from slice data in PrusaSlicer. Printing operating costs for the FDM printer would be calculated, which depend on labour, electricity, area rent and depreciation costs.

The machine hourly late for the Prusa i3 MK3S+ 3D printer can be calculated:

$$MHR = \frac{S_{dep}+S_{int}+S_{are}+S_{ene}+S_{per}}{MWT}, \tag{5}$$

where: MHR – machine hourly rate (Eur); S_{dep} – depreciation (Eur/year); S_{int} – interest (Eur/year); S_{are} – occupancy cost (Eur/year); S_{ene} – energy cost (Eur/year); S_{per} – employee costs (Eur/year).

$$S_{dep} = \frac{procurement\ value}{Service\ life\ in\ years}, \tag{6}$$

$$S_{int} == \frac{\frac{2}{3} \cdot procurement\ value, Eur \cdot interest}{100\%}, \tag{7}$$

$$S_{are} = Area\ cost \cdot 12\ months \cdot space\ req, \tag{8}$$

$$S_{ene} = Power \cdot Efficiency, \% \cdot energy\ costs\ \frac{Eur}{kWh} \cdot MWT, \tag{9}$$

$$S_{per} = Employee\ cost\ per\ h, Eur \cdot MWT, \tag{10}$$

The following values were inserted: procurement value – 849 (Eur), service life – 3 (years), efficiency – 90%, energy costs – 0.1497 (Eur/kWh), MWT (machine work time) – 1825 hours, employee cost per hour – 9.82 Eur, power consumption – 0.08 (W), required space – 1.764×10^{-2} (m^2) .

Procurement value was taken as the base price for the Prusa i3 MK3S+ 3D printer. The service life was taken from the fact that, the Prusa Research manufacturer provides a 1-year warranty for their printers, which can be extended to 2 or 3 years by purchasing an extended warranty. However, the actual lifespan of the printer can vary depending on factors such as usage, maintenance, and environmental conditions. Energy costs were taken as the average cost for first half of 2022 in Lithuania [74]. Machine work time was taken as the number of work time hours per year in Lithuania. Employee cost per hour was extracted as the average salary for 3D printing engineers in Lithuania.

Inserting the involved values into the before denoted equations, the machine hourly rate cane be calculated:

$$MHR = \frac{S_{dep}+S_{int}+S_{are}+S_{ene}+S_{per}}{MWT} = \frac{283+16.98+19.8+49.67+17921.5}{1825} \approx 10\ Eur/hour, \tag{11}$$

Since the purchased 1 kg of PLA filament costed 16.90 Eur, it can be assumed that 1 g of PLA costs ~0.02 Eur.

Cost of material, printing costs were calculated for each structure, Eq. 5 – Eq. 10 were inserted into Eq. 11. The resulting data was inserted into Table 11. The total costs were then divided by maximum achieved compressive strength, to indicate cost versus strength gained.

Table 11. Total cost for each printed part

Model	Used material, g	Est. printing time, min	Printing cost, €	Material cost, €	Total costs, €	Cost per strength
A1	3.85	63	10.51	0.07	10.57	3.62
A2	6.59	97	16.18	0.11	16.29	2.04
A3	10.52	131	21.85	0.18	22.02	2.16
A4	12.79	165	27.52	0.22	27.73	1.47
A5	17.46	199	33.19	0.30	33.48	1.09
H1	3.02	58	9.67	0.05	9.72	3.80
H2	4.91	72	12.01	0.08	12.09	3.15
H3	7.32	96	16.05	0.12	16.18	2.62
H4	9.64	129	21.51	0.16	21.68	1.60
H5	12.46	153	25.56	0.21	25.77	1.74

Judging from the resulting data and highlighting it via graph form in Fig. 40, it can be deducted that thinnest auxetic structure A1 has a relatively comparable price point to the corresponding hexagonal structure H1. For the second iteration the cost-effectiveness was indicated to drop significantly for the be relatively similar, as the cost for the A2 structure was drastically higher than that of H2. The quick rise of total cost for both models in the third iteration can be explained by analysing the initial printing setup. The slice preview indicated that when compared to the first and second iteration, the third and latter ones started using increasingly more layers to produce the parts. Final iterations H5 and A1, show a cost per strength of 1.74 and 1.09 accordingly.
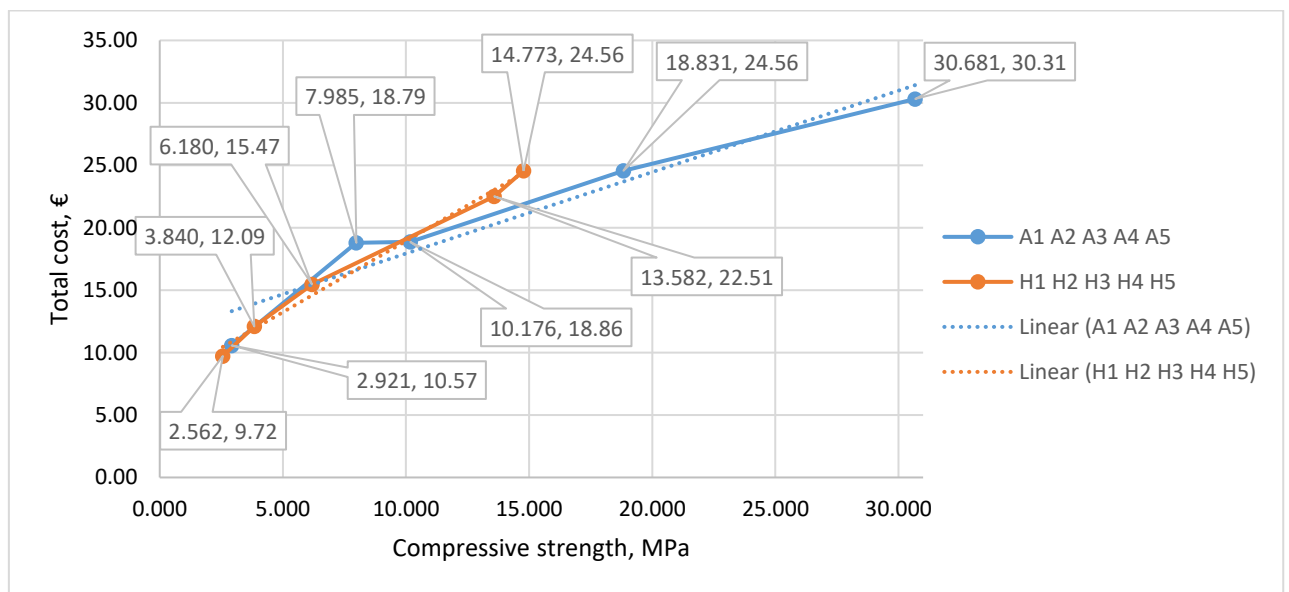
Fig. 40. Cost versus maximum compressive strength of auxetic and hexagonal models
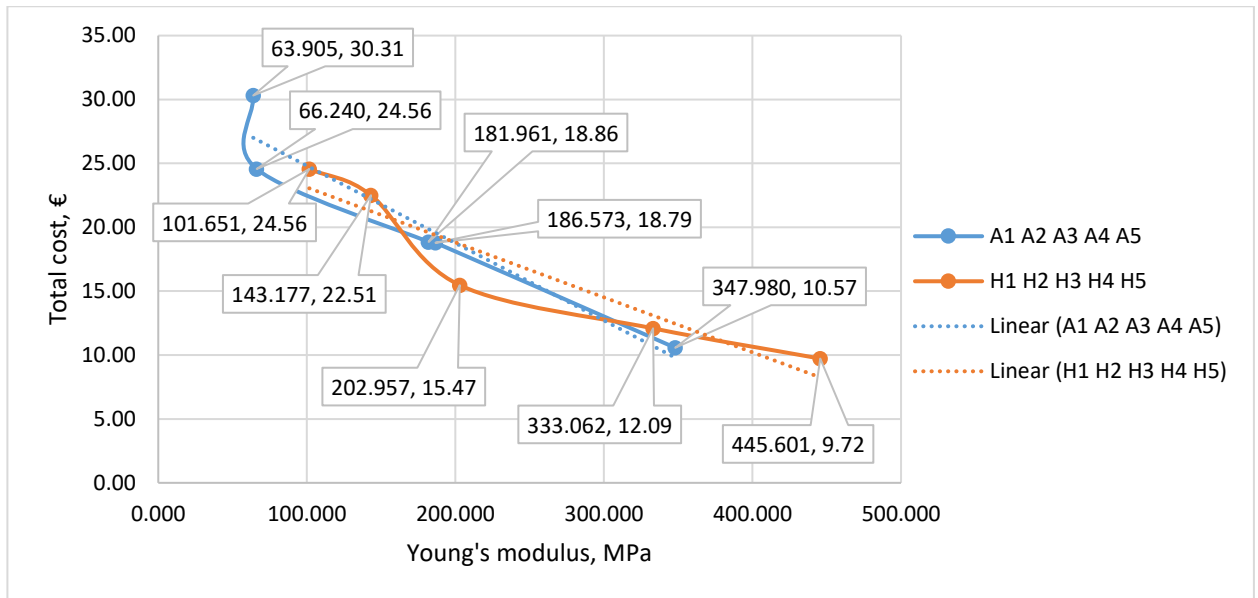
Fig. 41. Cost versus Young's modulus of auxetic and hexagonal models
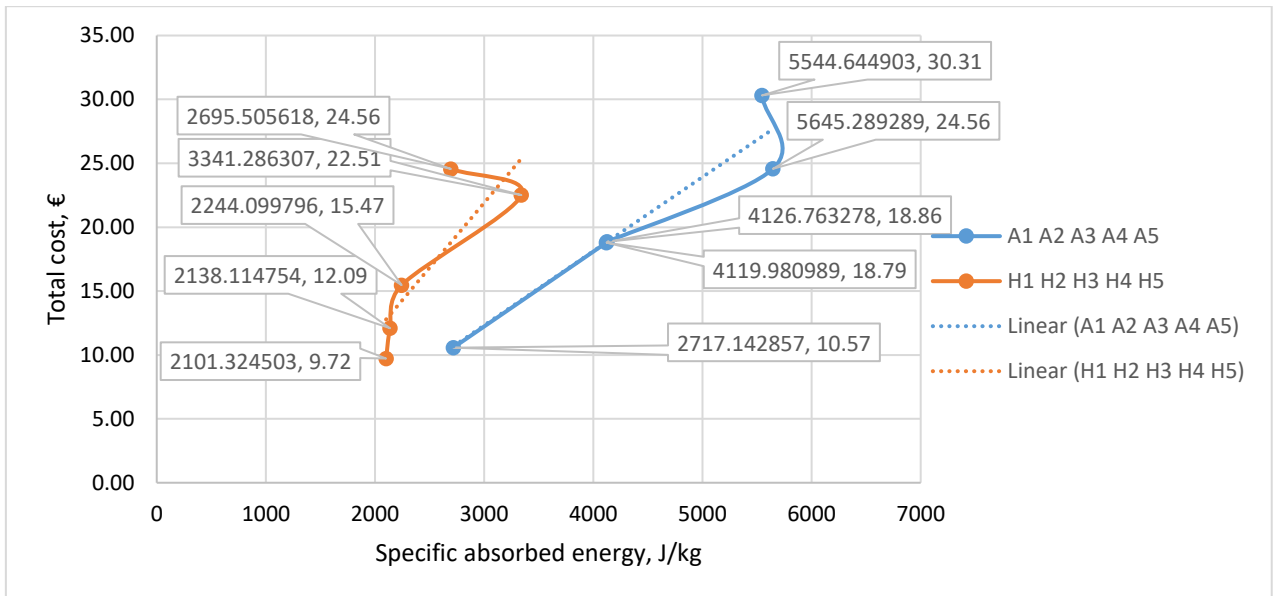
Fig. 42. Cost versus specific absorbed energy of auxetic and hexagonal models

Cost versus Young's modulus and versus specific absorbed energy are depicted indicated in Fig. 41. And Fig. 42 . A steeper trend of cost per Young's modulus can be seen for the auxetic group, this is due to the hexagonal models demonstrating higher stiffness overall. A bigger contrast between the models is seen in Fig. 41, as hexagonal models show a trend of increased cost with no relative specific absorbed energy gained.

4.1. Summary of Economic Benefits of Printing NPR Structures

Overall, a lower total cost per compression strength gained ratio of auxetic models indicate that the structure on average based on wall thickness is more cost-effective than its counterpart. With final iterations of the model indicating a cost per strength of 1.74 and 1.09 accordingly for hexagonal and auxetic structures. This would mean that producing components or structures using 3D printing, injection molding, or other manufacturing processes, using auxetic structures could lead to lower

material and manufacturing costs. By using the more cost-effective re-entrant structure, more components or parts could be produced within a given budget, thereby improving efficiency and reducing waste. Additionally, it would be possible to explore more design possibilities and iterations without exceeding budget constraints. This could lead to more innovative and optimized designs. As a result, products and services using these optimizations would yield lower cost than that of a competitor, which could increase one' competitiveness and market share.

For any construction, the scalability and accessibility of the production methods and materials should be taken into account. A wider variety of readily accessible materials and tried-and-true production methods may be advantageous for hexagonal constructions, lowering prices. Auxetic structures, particularly those with complicated geometries or specialty materials, may have scaling and supply issues that might affect how cost-effective they are. The project compared relatively geometrically similar models, complications could arise, if more complex auxetic structures such as chiral or rotating polygon models were under investigation, since they are considered for their more complex geometry. However, it is important to consider that both structures show relatively parallel cost-effectiveness, considering compression strength and Young's modulus. On average, the gained mechanical properties of hexagonal models not only start to diminish per iteration, but also hit a certain limit when compared to the auxetic structures.

Conclusions

1. Materials and structures with a negative Poisson's ratio are commonly used in construction, aerospace, medicine, sports due to their passive energy absorption and dissipation. Most research has focused on the structural qualities and mechanical benefits of auxetic materials.

2. Comparison of 3D printable auxetic structures has led to the discovery of various patterns, including chiral, re-entrant, and rotating polygon structures, which offer unique mechanical properties. The hexagonal re-entrant model demonstrated unique mechanical behaviour and was selected for further investigation in future experiments.

3. Average compression results showed that the auxetic structures had lower Young's moduli than the hexagonal ones – 169.332 MPa compared to 245.29 MPa, which indicated their ability to deform more easily. The average compressive strength of the auxetic structures was higher than that of the hexagonal ones – 14.119 MPa compared to 8.187 MPa, which meant that they could withstand more force before failure.

4. Auxetic structures show a trendline of improving cost-effectiveness, with the final value of 1.09 compared to the hexagonal –1.74. The findings suggest that the re-entrant structure of auxetics can lead to lower material and manufacturing costs while still maintaining high compressive strength.

List of References

1. YUAN, X., et al. Recent Progress in the Design and Fabrication of Multifunctional Structures Based on Metamaterials. *Current Opinion in Solid State & Materials Science*, Feb, 2021, vol. 25, no. 1. pp. 100883. Available from: https://dx.doi.org/10.1016/j.cossms.2020.100883 CrossRef. ISSN 1359-0286. DOI 10.1016/j.cossms.2020.100883.

2. TAHIR, D., ZHANG, M. and HU, H. Auxetic Materials for Personal Protection: A Review. *Physica Status Solidi. B, Basic Solid State Physics*, Dec, 2022, vol. 259, no. 12. pp. 2200324-n/a. Available from: https://onlinelibrary.wiley.com/doi/abs/10.1002/pssb.202200324 CrossRef. ISSN 0370-1972. DOI 10.1002/pssb.202200324.

3. GU, G.X., TAKAFFOLI, M. and BUEHLER, M.J. *Hierarchically Enhanced Impact Resistance of Bioinspired Composites.* Wiley, -05-26, 2017 ISBN 0935-9648. DOI 10.1002/adma.201700060.

4. ROSS, A.G., DONALDSON, A. and POULOS, R.G. Nationwide Sports Injury Prevention Strategies: A Scoping Review. *Scandinavian Journal of Medicine & Science in Sports*, Feb, 2021, vol. 31, no. 2. pp. 246-264. Available from: https://onlinelibrary.wiley.com/doi/abs/10.1111/sms.13858 MEDLINE. ISSN 0905-7188. DOI 10.1111/sms.13858.

5. *Trail Skins Air Knee Guard.* , 2023 [viewed March 13, 2023]. Available from:/accessories-c11/protective-gear-c192/dainese-trail-skins-air-knee-guard-p43069.

6. L. FANATIC. *ECD Echo Lacrosse Arm Pads.* , 2023 [viewed March 13, 2023]. Available from:https://lacrossefanatic.com/products/ecd-echo-lacrosse-arm-pads.

7. DING, W. Experimental Analysis of Superplastic Deformation of Titanium Alloy Based on Sports Equipment. *Integrated Ferroelectrics*, Jul 24, 2022, vol. 227, no. 1. pp. 257-272. Available from: https://www.tandfonline.com/doi/abs/10.1080/10584587.2022.2072115 CrossRef. ISSN 1058-4587. DOI 10.1080/10584587.2022.2072115.

8. WU, Q., et al. Computational Studies of Porous Head Protection Structures for Human Cranium Under Impact Loading. *Acta Mechanica Solida Sinica*, Aug 01, 2021, vol. 34, no. 4. pp. 477-493. Available from: https://link.springer.com/article/10.1007/s10338-021-00222-2 CrossRef. ISSN 0894-9166. DOI 10.1007/s10338-021-00222-2.

9. HUANG, X., et al. Flexible Mechanical Metamaterials Enabled Electronic Skin for Real-Time Detection of Unstable Grasping in Robotic Manipulation. *Advanced Functional Materials*, Jun 03, 2022, vol. 32, no. 23. pp. 2109109-n/a. Available from: https://onlinelibrary.wiley.com/doi/abs/10.1002/adfm.202109109 CrossRef. ISSN 1616-301X. DOI 10.1002/adfm.202109109.

10. NAGELLI, C., et al. *Mechanical and Possible Auxetic Properties of Human Achilles Tendon during in Vitro Testing to Failure.* Cold Spring Harbor: Cold Spring Harbor Laboratory Press. Sep 10, 2021 Available from: https://search.proquest.com/docview/2571339902 Publicly Available Content Database. DOI 10.1101/2021.09.09.459526.

11. SHUKLA, S. and BEHERA, B.K. Auxetic Fibrous Materials and Structures in Medical Engineering - a Review. *The Journal of the Textile Institute*, Aug 22, 2022, vol. ahead-of-print, no. ahead-of-print. pp. 1-12. Available from: https://www.tandfonline.com/doi/abs/10.1080/00405000.2022.2116549 CrossRef. ISSN 0040-5000. DOI 10.1080/00405000.2022.2116549.

12. MARDLING, P., ALDERSON, A., JORDAN-MAHY, N. and LE MAITRE, C.L. The use of Auxetic Materials in Tissue Engineering. *Biomaterials Science*, Apr 21, 2020, vol. 8, no. 8. pp.

274-283. Available from: https://www.ncbi.nlm.nih.gov/pubmed/32215398 PubMed. ISSN 2047-4830. DOI 10.1039/c9bm01928f.

13. PASCUAL, G., et al. Behaviour of a New Composite Mesh for the Repair of Full-Thickness Abdominal Wall Defects in a Rabbit Model. *PLoS ONE*, Nov 13, 2013, vol. 8, no. 11. pp. e80647. Available from: https://www.ncbi.nlm.nih.gov/pubmed/24236192 MEDLINE. ISSN 1932-6203. DOI 10.1371/journal.pone.0080647.

14. Zadpoor Amir. *Researchers Develop Hybrid Meta-Biomaterial that can Prolong Lifespan of Hip Implants.* Jan 3, 2018 [viewed March 13, 2023]. Available from:https://phys.org/news/2018-01-hybrid-meta-biomaterial-prolong-lifespan-hip.html.

15. GHAVIDELNIA, N., BODAGHI, M. and HEDAYATI, R. Femur Auxetic Meta-Implants with Tuned Micromotion Distribution. *Materials*, Jan 01, 2021, vol. 14, no. 1. pp. 114. Available from: https://www.narcis.nl/publication/RecordID/oai:tudelft.nl:uuid:48743397-6ed5-48ca-99df-5747cd0eec06 PubMed. ISSN 1996-1944. DOI 10.3390/ma14010114.

16. CHOW, L., et al. 3D Printing Auxetic Architectures for Hypertrophic Scar Therapy. *Macromolecular Materials and Engineering*, May, 2022, vol. 307, no. 5. pp. 2100866-n/a. Available from: https://onlinelibrary.wiley.com/doi/abs/10.1002/mame.202100866 CrossRef. ISSN 1438-7492. DOI 10.1002/mame.202100866.

17. DIKICI, Y., et al. *Piece-By-Piece Shape-Morphing: Engineering Compatible Auxetic and Non-Auxetic Lattices to Improve Soft Robot Performance in Confined Spaces.* Wiley, -03-31, 2022 ISBN 1438-1656. DOI 10.1002/adem.202101620.

18. LEE, Y., et al. Tendon-Driven Auxetic Tubular Springs for Resilient Hopping Robots. *Advanced Intelligent Systems*, Apr, 2022, vol. 4, no. 4. pp. 2100152-n/a. Available from: https://onlinelibrary.wiley.com/doi/abs/10.1002/aisy.202100152 CrossRef. ISSN 2640-4567. DOI 10.1002/aisy.202100152.

19. SHINTAKE, J., NAGAI, T. and OGISHIMA, K. Sensitivity Improvement of Highly Stretchable Capacitive Strain Sensors by Hierarchical Auxetic Structures. *Frontiers in Robotics and AI*, Nov 22, 2019, vol. 6. pp. 127. Available from: https://www.ncbi.nlm.nih.gov/pubmed/33501142 PubMed. ISSN 2296-9144. DOI 10.3389/frobt.2019.00127.

20. HAN, Y. and LU, W.F. Structural Design of Wearable Electronics Suitable for Highly-Stretched Joint Areas. *Smart Materials and Structures*, Oct 01, 2018, vol. 27, no. 10. pp. 105042. Available from: https://iopscience.iop.org/article/10.1088/1361-665X/aadf05 CrossRef. ISSN 0964-1726. DOI 10.1088/1361-665X/aadf05.

21. ATTARD, D., CASHA, A.R. and GRIMA, J.N. *Filtration Properties of Auxetics with Rotating Rigid Units.* MDPI AG, -05-03, 2018 DOI 10.3390/ma11050725.

22. ALDERSON, A., RASBURN, J. and EVANS, K.E. Mass Transport Properties of Auxetic (Negative Poisson's Ratio) Foams. *Physica Status Solidi (B)*, Mar, 2007, vol. 244, no. 3. pp. 817-827. Available from: https://api.istex.fr/ark:/67375/WNG-7N6XWGCC-9/fulltext.pdf CrossRef. ISSN 0370-1972. DOI 10.1002/pssb.200572701.

23. DUBROVSKI, P.D., et al. In-Plane Deformation Behavior and the Open Area of Rotating Squares in an Auxetic Compound Fabric. *Polymers*, Jan 31, 2022, vol. 14, no. 3. pp. 571. Available from: https://www.ncbi.nlm.nih.gov/pubmed/35160560 PubMed. ISSN 2073-4360. DOI 10.3390/polym14030571.

24. BISWAS, A.N., et al. Hybrid Auxetic Materials Implemented in Crates & Non-Pneumatic Wheels for Shock Absorption. *Materials Today : Proceedings*, 2022, vol. 56. pp. 1327-1334. Available

from: https://dx.doi.org/10.1016/j.matpr.2021.11.326 CrossRef. ISSN 2214-7853. DOI 10.1016/j.matpr.2021.11.326.

25. BIHARTA, M.A.S., SANTOSA, S.P. and WIDAGDO, D. Design and Optimization of Lithium-Ion Battery Protector with Auxetic Honeycomb for in-Plane Impact using Machine Learning Method. *Frontiers in Energy Research*, Feb 01, 2023, vol. 11. Available from: https://doaj.org/article/8cb96c04e89b4ab4a12f372191995cc5 CrossRef. ISSN 2296-598X. DOI 10.3389/fenrg.2023.1114263.

26. HUO, S., GAO, Z. and RUAN, D. Crashworthiness of a Hybrid Tube with an Auxetic Layer. *Engineering Failure Analysis*, Dec, 2022, vol. 142. pp. 106755. Available from: https://dx.doi.org/10.1016/j.engfailanal.2022.106755 CrossRef. ISSN 1350-6307. DOI 10.1016/j.engfailanal.2022.106755.

27. BUDARAPU, P.R., Y B, S.S. and NATARAJAN, R. Design Concepts of an Aircraft Wing：Composite and Morphing Airfoil with Auxetic Structures. *Frontiers of Structural and Civil Engineering*, Dec 01, 2016, vol. 10, no. 4. pp. 394-408. Available from: http://lib.cqvip.com/qk/71754X/201604/670766705.html CrossRef. ISSN 2095-2430. DOI 10.1007/s11709-016-0352-z.

28. SUN, J., GUAN, Q., LIU, Y. and LENG, J. *Morphing Aircraft Based on Smart Materials and Structures: A State-of-the-Art Review.* London, England: SAGE Publications, Oct 01, 2016 Available from: https://journals.sagepub.com/doi/full/10.1177/1045389X16629569 CrossRef. ISBN 1045-389X. DOI 10.1177/1045389X16629569.

29. VOCKE, R.D., KOTHERA, C.S., WOODS, B.K.S. and WERELEY, N.M. Development and Testing of a Span-Extending Morphing Wing. *Journal of Intelligent Material Systems and Structures*, Jun, 2011, vol. 22, no. 9. pp. 879-890. Available from: https://journals.sagepub.com/doi/full/10.1177/1045389X11411121 CrossRef. ISSN 1045-389X. DOI 10.1177/1045389X11411121.

30. ZHANG, K., et al. Ultrahigh Energy-Dissipation and Multifunctional Auxetic Polymeric Foam Inspired by Balloon Art. *Composites. Part A, Applied Science and Manufacturing*, Apr, 2023, vol. 167. pp. 107435. Available from: https://dx.doi.org/10.1016/j.compositesa.2023.107435 CrossRef. ISSN 1359-835X. DOI 10.1016/j.compositesa.2023.107435.

31. TAFRIHI, E. and ABDEL-RAHMAN, A. *Heat-Actuated Auxetic Facades.* , -07, 2018.

32. EDGAR, J. and TINT, S. Additive Manufacturing Technologies: 3D Printing, Rapid Prototyping, and Direct Digital Manufacturing, 2nd Edition. *Johnson Matthey Technology Review*, Jul 01, 2015, vol. 59, no. 3. pp. 193-198. Available from: https://www.ingentaconnect.com/content/matthey/jmtr/2015/00000059/00000003/art00004 CrossRef. ISSN 2056-5135. DOI 10.1595/205651315X688406.

33. KIM, J., MAHATO, M., OH, J. and OH, I. Multi-Purpose Auxetic Foam with Honeycomb Concave Micropattern for Sound and Shock Energy Absorbers. *Advanced Materials Interfaces*, Feb 03, 2023, vol. 10, no. 4. pp. n/a. Available from: https://onlinelibrary.wiley.com/doi/abs/10.1002/admi.202202092 Materials Research Database. ISSN 2196-7350. DOI 10.1002/admi.202202092.

34. HAN, D., et al. Lightweight Auxetic Metamaterials: Design and Characteristic Study. *Composite Structures*, Aug 01, 2022, vol. 293. pp. 115706. Available from: https://dx.doi.org/10.1016/j.compstruct.2022.115706 CrossRef. ISSN 0263-8223. DOI 10.1016/j.compstruct.2022.115706.

35. HUANG, H., WONG, B. and CHOU, Y. Design and Properties of 3D-Printed Chiral Auxetic Metamaterials by Reconfigurable Connections. *Physica Status Solidi. B, Basic Solid State Physics*, Aug, 2016, vol. 253, no. 8. pp. 1557-1564. Available from: https://api.istex.fr/ark:/67375/WNG-L2D6XL65-L/fulltext.pdf Technology Research Database. ISSN 0370-1972. DOI 10.1002/pssb.201600027.

36. ORHAN, S.N. and ERDEN, Ş. Numerical Investigation of the Mechanical Properties of 2D and 3D Auxetic Structures. *Smart Materials and Structures*, Jun 01, 2022, vol. 31, no. 6. pp. 65011 CrossRef. ISSN 0964-1726. DOI 10.1088/1361-665X/ac6918.

37. YU, L., TAN, H. and ZHOU, Z. Mechanical Properties of 3D Auxetic Closed-Cell Cellular Structures. *International Journal of Mechanical Sciences*, Jul 01, 2020, vol. 177. pp. 105596. Available from: https://dx.doi.org/10.1016/j.ijmecsci.2020.105596 CrossRef. ISSN 0020-7403. DOI 10.1016/j.ijmecsci.2020.105596.

38. GUO, M., YANG, H. and MA, L. 3D Lightweight Double Arrow-Head Plate-Lattice Auxetic Structures with Enhanced Stiffness and Energy Absorption Performance. *Composite Structures*, Jun 15, 2022, vol. 290. pp. 115484. Available from: https://dx.doi.org/10.1016/j.compstruct.2022.115484 CrossRef. ISSN 0263-8223. DOI 10.1016/j.compstruct.2022.115484.

39. CARTION, M.A. and GANTER, M. *Fast and Simple Printing of Graded Auxetic Structures.* IEEE, -06, 2013 DOI 10.1109/cbmi.2013.6576567.

40. Schreiber A. Barbara. *3D Printing | Definition, Technology, History, & Applications | Britannica.* , 2023 [viewed Apr 20, 2023]. Available from:https://www.britannica.com/technology/3D-printing.

41. WANG, X., WANG, B., LI, X. and MA, L. Mechanical Properties of 3D Re-Entrant Auxetic Cellular Structures. *International Journal of Mechanical Sciences*, Oct, 2017, vol. 131-132. pp. 396-407. Available from: https://dx.doi.org/10.1016/j.ijmecsci.2017.05.048 CrossRef. ISSN 0020-7403. DOI 10.1016/j.ijmecsci.2017.05.048.

42. HAZRAT ALI, M., BATAI, S. and KARIM, D. Material Minimization in 3D Printing with Novel Hybrid Cellular Structures. *Materials Today : Proceedings*, 2021, vol. 42. pp. 1800-1809. Available from: https://dx.doi.org/10.1016/j.matpr.2020.12.185 CrossRef. ISSN 2214-7853. DOI 10.1016/j.matpr.2020.12.185.

43. INGROLE, A., HAO, A. and LIANG, R. Design and Modeling of Auxetic and Hybrid Honeycomb Structures for in-Plane Property Enhancement. *Materials & Design*, Mar 05, 2017, vol. 117. pp. 72-83. Available from: https://dx.doi.org/10.1016/j.matdes.2016.12.067 CrossRef. ISSN 0264-1275. DOI 10.1016/j.matdes.2016.12.067.

44. CHANGFANG, Z., et al. Compressive Mechanical Behavior for Surface Auxetic Structures. *Journal of Alloys and Compounds*, Feb 15, 2022, vol. 894. pp. 162427. Available from: https://dx.doi.org/10.1016/j.jallcom.2021.162427 CrossRef. ISSN 0925-8388. DOI 10.1016/j.jallcom.2021.162427.

45. PRAWOTO, Y. and TAMIN, M.N. A New Direction in Computational Fracture Mechanics in Materials Science: Will the Combination of Probabilistic and Fractal Fracture Mechanics Become Mainstream?. *Computational Materials Science*, Mar 01, 2013, vol. 69. pp. 197-203. Available from: https://dx.doi.org/10.1016/j.commatsci.2012.11.018 CrossRef. ISSN 0927-0256. DOI 10.1016/j.commatsci.2012.11.018.

46. TANG, H., et al. Highly Tailorable Electromechanical Properties of Auxetic Piezoelectric Ceramics with Ultra-low Porosity. *Journal of the American Ceramic Society*, Nov, 2020, vol. 103, no. 11. pp. 6330-6347. Available from: https://onlinelibrary.wiley.com/doi/abs/10.1111/jace.17356 CrossRef. ISSN 0002-7820. DOI 10.1111/jace.17356.

47. GRIMA, J.N. and EVANS, K.E. Auxetic Behavior from Rotating Squares. *Journal of Materials Science*, May 01, 2006, vol. 41, no. 10. pp. 3193-3196. Available from: https://search.proquest.com/docview/2259703377 CrossRef. ISSN 0022-2461. DOI 10.1007/s10853-006-6339-8.

48. REN, X., et al. *Auxetic Metamaterials and Structures: A Review.* IOP Publishing, -01-24, 2018 ISBN 0964-1726. DOI 10.1088/1361-665x/aaa61c.

49. SHAN, S., et al. Design of Planar Isotropic Negative Poisson's Ratio Structures. *Extreme Mechanics Letters*, Sep 01, 2015, vol. 4. pp. 96-102 CrossRef. ISSN 2352-4316. DOI 10.1016/j.eml.2015.05.002.

50. MAZUR, E. and SHISHKOVSKY, I. Additively Manufactured Hierarchical Auxetic Mechanical Metamaterials. *Materials*, Aug 15, 2022, vol. 15, no. 16. pp. 5600. Available from: https://search.proquest.com/docview/2706251362 CrossRef. ISSN 1996-1944. DOI 10.3390/ma15165600.

51. DUDEK, K.K., et al. *On the Dynamics and Control of Mechanical Properties of Hierarchical Rotating Rigid Unit Auxetics.* Springer Science and Business Media LLC, -04-26, 2017 DOI 10.1038/srep46529.

52. LIANG, Y., et al. Research on the Auxetic Behavior and Mechanical Properties of Periodically Rotating Graphene Nanostructures. *Nanotechnology Reviews (Berlin)*, Apr 21, 2022, vol. 11, no. 1. pp. 1733-1743. Available from: http://www.degruyter.com/doi/10.1515/ntrev-2022-0098 CrossRef. ISSN 2191-9097. DOI 10.1515/ntrev-2022-0098.

53. MUSTAHSAN, F., et al. Re-Entrant Honeycomb Auxetic Structure with Enhanced Directional Properties. *Materials*, Nov 14, 2022, vol. 15, no. 22. pp. 8022. Available from: https://www.ncbi.nlm.nih.gov/pubmed/36431508 PubMed. ISSN 1996-1944. DOI 10.3390/ma15228022.

54. JIANG, Y. and LI, Y. 3D Printed Auxetic Mechanical Metamaterial with Chiral Cells and Re-Entrant Cores. *Scientific Reports*, Feb 05, 2018, vol. 8, no. 1. pp. 2397-11. Available from: https://www.ncbi.nlm.nih.gov/pubmed/29402940 MEDLINE. ISSN 2045-2322. DOI 10.1038/s41598-018-20795-2.

55. LOGAKANNAN, K.P., RAMACHANDRAN, V., RENGASWAMY, J. and RUAN, D. Stiffened Star-Shaped Auxetic Structure with Tri-Directional Symmetry. *Composite Structures*, Jan 01, 2022, vol. 279. pp. 114773. Available from: https://dx.doi.org/10.1016/j.compstruct.2021.114773 CrossRef. ISSN 0263-8223. DOI 10.1016/j.compstruct.2021.114773.

56. GAO, Y., et al. Composite Tree-Like Re-Entrant Structure with High Stiffness and Controllable Elastic Anisotropy. *International Journal of Solids and Structures*, Dec 01, 2020, vol. 206. pp. 170-182. Available from: https://dx.doi.org/10.1016/j.ijsolstr.2020.09.003 CrossRef. ISSN 0020-7683. DOI 10.1016/j.ijsolstr.2020.09.003.

57. MOUSANEZHAD, D., et al. Elastic Properties of Chiral, Anti-Chiral, and Hierarchical Honeycombs：A Simple Energy-Based Approach. *Theoretical and Applied Mechanics Letters*, Mar 01, 2016, vol. 6, no. 2. pp. 81-96. Available from:

http://lib.cqvip.com/qk/71275X/201602/668763237.html CrossRef. ISSN 2095-0349. DOI 10.1016/j.taml.2016.02.004.

58. GRIMA, J.N., GATT, R. and FARRUGIA, P. On the Properties of Auxetic Meta-Tetrachiral Structures. *Physica Status Solidi (B)*, Mar, 2008, vol. 245, no. 3. pp. 511-520. Available from: https://api.istex.fr/ark:/67375/WNG-PB58XFNP-L/fulltext.pdf CrossRef. ISSN 0370-1972. DOI 10.1002/pssb.200777704.

59. MIZZI, L., et al. *An Analytical and Finite Element Study on the Mechanical Properties of Irregular Hexachiral Honeycombs.* IOP Publishing, -09-05, 2018 ISBN 0964-1726. DOI 10.1088/1361-665x/aad3f6.

60. POZNIAK, A.A. and WOJCIECHOWSKI, K.W. Poisson's Ratio of Rectangular Anti-Chiral Structures with Size Dispersion of Circular Nodes. *Physica Status Solidi (B)*, Feb, 2014, vol. 251, no. 2. pp. 367-374 CrossRef. ISSN 0370-1972. DOI 10.1002/pssb.201384256.

61. DESTEFANO, V., KHAN, S. and TABADA, A. Applications of PLA in Modern Medicine. *Engineered Regeneration*, 2020, vol. 1. pp. 76-87. Available from: https://dx.doi.org/10.1016/j.engreg.2020.08.002 CrossRef. ISSN 2666-1381. DOI 10.1016/j.engreg.2020.08.002.

62. FARAH, S., ANDERSON, D.G. and LANGER, R. Physical and Mechanical Properties of PLA, and their Functions in Widespread Applications — A Comprehensive Review. *Advanced Drug Delivery Reviews*, Dec 15, 2016, vol. 107. pp. 367-392. Available from: https://dx.doi.org/10.1016/j.addr.2016.06.012 PubMed. ISSN 0169-409X. DOI 10.1016/j.addr.2016.06.012.

63. WANG, T., WANG, L., MA, Z. and HULBERT, G.M. Elastic Analysis of Auxetic Cellular Structure Consisting of Re-Entrant Hexagonal Cells using a Strain-Based Expansion Homogenization Method. *Materials & Design*, Dec 15, 2018, vol. 160. pp. 284-293. Available from: https://dx.doi.org/10.1016/j.matdes.2018.09.013 CrossRef. ISSN 0264-1275. DOI 10.1016/j.matdes.2018.09.013.

64. BITZER, T.N. *Honeycomb Technology: Materials, Design, Manufacturing, Applications and Testing.* Springer, Dec 6, 2012 ISBN 9780412540509.

65. Re-Entrant 2D PyAuxetic 2.0.1 Documentation, 2021 [viewed May 7, 2023]. Available from: https://pyauxetic.mkhoshbin.com/en/latest/unit-cell-library/reentrant2d.html.

66. KIM, Y., Son Kukhui and Lee Jinwoo. *Auxetic_Structures_for_Tissue_Engineering_Scaffold.* Nov 12, 2021.

67. International Organization for Standardization. *ISO 604:2002(En), Plastics Determination of Compressive Properties.* , 2002 [viewed Apr 19, 2023]. Available from: https://www.iso.org/obp/ui/#iso:std:iso:604:ed-3:v1:en.

68. *Original Prusa I3 MK3S+ 3D Printer | Original Prusa 3D Printers Directly from Josef Prusa.* , 2023 [viewed Feb 7, 2023]. Available from:https://www.prusa3d.com/product/original-prusa-i3-mk3s-3d-printer-3/#specs.

69. *Pla 1kg.* , 2023 [viewed Mar 8, 2023]. Available from:https://filalab.shop/en/home/pla-1kg.html.

70. *Tinius Olsen H25KT.* , 2023.

71. FRANCISCO, M.B., et al. *Multiobjective Design Optimization of Reentrant Auxetic Model using Lichtenberg Algorithm Based on Metamodel.* Research Square Platform LLC, -01-10, 2022 DOI 10.21203/rs.3.rs-1225593/v1.

72. LU, G. and YU, T.X. *Energy Absorption of Structures and Materials.* Boca Raton: CRC Press, 2003 ISBN 1855738589.

73. ALDERSON, K.L. and EVANS, K.E. *Auxetic Materials: The Positive Side of being Negative.* , Aug 1, 2000 CrossRef.

74. *Electricity Price Statistics.* , 2023 [viewed Apr 8, 2023]. Available from:https://ec.europa.eu/eurostat/statistics-explained/index.php?title=Electricity_price_statistics.